HEATING OF MAGNETIZED PLASMAS BY A LARGE-AMPLITUDE LOW-FREQUENCY ELECTRIC FIELD

By

Liu Chen and C.K. Birdsall

Memorandum No. ERL-M352

June 1972

ELECTRONICS RESEARCH LABORATORY

College of Engineering
University of California, Berkeley
94720

Liu Chen is presently at the Bell Telephone Labs., Murray Hill, N.J.

Research sponsored by the Atomic Energy Commission, Contract AT(04-3)-34, Project 128.

ABSTRACT

Plasma electron and ion heating due to a large-amplitude oscillating electric field E_o applied normal to a steady magnetic field B_o has been followed in detail, by one-dimensional computer simulations. The large oscillating drift velocity ($E_o/B_o > v_e$) at low frequency ($\omega_{ci} << \omega_o \simeq \omega_{pi} << \omega_{ce}$) sets up instabilities due to the periodic electron E/B drift through the ions, which then cause rapid heatings. For waves propagating across $\vec{B}_o$ ($\vec{k}\cdot\hat{B}_o = k_{||} = 0$), the instability is a Buneman-type upper-hybrid two-stream instability. Electron perpendicular thermal velocity is increased to $\sim E_o/B_o$ with little ion heating. For obliquely propagating waves ($k_{||} \neq 0$), there is an additional instability, the modified two-stream instability. For small $k_{||}$ (roughly, $k_{||}/k \lesssim \sqrt{m_e/m_i}$), the upper-hybrid instability dominates and the heating is similar to the $k_{||} = 0$ case but with a small amount of electron parallel heating. As $k_{||}$ increases, however, the modified two-stream instability becomes dominant. Electron parallel thermal velocity is increased to $\simeq (E_o/B_o)(k/k_{||})$. Strong ion (perpendicular) heating also occurs with the ion thermal velocity at wave saturation near $(E_o/B_o)(m_e/m_i)^{3/4}(k/k_{||})^{3/2}$. Comparison with similar work with $B_o = 0$ shows that addition of B_o is best for ion heating, improving KT_i by $(m_i/m_e)^{1/2}$. Possible applications of these results to laboratory experiments are also discussed.

I. INTRODUCTION

Many currently employed as well as proposed future plasma heating schemes often involve an oscillating electric field applied across the confining magnetic field. Hence there has been considerable interest in the large-amplitude, nonlinear behavior of such plasmas. Using one-dimensional (x, v_x, v_y, v_z) computer simulation, we have studied this problem and the results of our investigations are presented in this paper.

The plasmas considered here have $\omega_{ce} \sim \omega_{pe} >> \omega_{pi} >> \omega_{ci}$ (with obvious notations for the electron and ion cyclotron frequencies and plasma frequencies). Electrons and ions have equal initial temperatures. The external electric field, $\vec{E}_{ext} = \vec{E}_o \sin \omega_o t$, is applied perpendicular to the magnetic field $\vec{B}_o$ and has driving frequency ω_o near ω_{pi}. Since $\omega_{ci} << \omega_{pi} \sim \omega_o << \omega_{ce}$ the electrons are strongly "magnetized" and their main motion is the $\vec{E}_{ext} \times \vec{B}_o$ oscillating drift with peak amplitude E_o/B_o. Ions, however, are effectively "unmagnetized" and mainly oscillate in the direction of $\vec{E}_{ext}$ with an amplitude $\frac{eE_o}{m_i\omega_o} = \frac{E_o}{B_o}\frac{\omega_{ci}}{\omega_o} << \frac{E_o}{B_o}$. Thus the dominant electron-ion relative motion is the electron $\vec{E} \times \vec{B}$ streaming through the ions. If the electron drift were steady and greater than some threshold value, then instabilities might be excited. With an oscillating drift therefore, we might expect the same kind of instability over a fraction of the cycle, during which the drift speed is greater

than the threshold value. The growth of this periodic-streaming instability may be accompanied by the increases in plasma temperatures and, hence, is the source of heating.

In our investigations, the applied electric field is of large amplitude so as to make E_o/B_o large compared with the initial electron thermal velocity v_e ; that is, we have $E_o/B_o\ v_e \simeq 5$ to 10. Two types of periodic-streaming non-resonant instabilities are observed in the simulations: (1) Buneman-type two-stream instability[9] with $k\ E_o/B_o \sim \omega_{UH} = (\omega_{pe}^2 + \omega_{ce}^2)^{1/2}$ and instability threshold near v_e, and (2) modified two-stream instability[13] with $k\ E_o/B_o \sim \omega_{pi}$ and instability threshold near v_i, which only occurs when the wave vector $\vec{k}$ has a non-zero component along $\vec{B}_o$. When the wave energy becomes large, strong plasma heating occurs. The observed heating processes depend critically on which type of instability is dominant.

Recently Okuda et al[1] have also investigated the plasma heatings caused by applying low-frequency electric field across the magnetic field. They, however, are mainly interested in parametric instabilities excited by a low-amplitude ($E_o/B_o v_e < 1$) pump field in contrast to our case where instabilities are due to drifts induced by a large-amplitude pump field and parametric effects are expected to be relatively small.

As an example of possible experimental configurations, we mention here the experiments of plasma (ion) heating by modulated electron beams[2-4], which partially motivated this research.

In these experiments, an electron beam, modulated near ω_{pi}, is injected into a mirror-confined plasma. In a simple view the electron beam can be represented by a charged thin line moving parallel to the magnetic field. The beam line charge then varies in time according to the prescribed modulation. Due to the lack of charge reservoir to neutralize the overall beam-plasma system, a radial electric field oscillating near ω_{pi} appears . This electric field then produces electron oscillating $\vec{E} \times \vec{B}$ drift in the azimuthal direction, while ions mainly oscillate in the radial direction. Another possible application is in microwave heating experiments. Further discussions relating our results and laboratory experiments are in the last Section.

The numerical simulation model is described in Section II. Section III contains the physical parameters of the simulations. We have systematically investigated the heating processes with respect to the applied field strength and the orientation of $\vec{k}$, and three representative simulation results are presented in Section IV. In Section V linear and nonlinear theories based on a steady drift and trapping arguments are developed to explain and compare with the simulation results. In Section VI, heating results with and without B_o are compared. The final conclusions and discussions are in Section VI.

II. SIMULATION MODEL

The numerical simulation model is illustrated in Fig. 1. $\vec{B}_o$ lies in the $\hat{z} - \hat{k}$ ($\hat{x}$) plane with an angle $\pi/2 - \theta$ between $\vec{B}_o$ and $\hat{k}$. $\theta \neq 0$ then allows $\vec{k}$ to have a component along $\vec{B}_o$; i.e., $k = \vec{k}.\vec{B}_o/B_o \neq 0$. The applied electric field E_o is in the $\hat{y}$ - direction normal to B_o. The self-consistent field of the ions and electrons is obtained from a CIC code, which is one-dimensional (x, v_x, v_y, v_z), electrostatic, with periodic boundary conditions[5]. The charge clouds (slabs) have nominal thickness equal to a cell length Δx. Charge density is known at the grid points and Poisson's equation is then solved numerically by the method of Discrete Fast Fourier Transform. Particles are advanced in time using "Cylrad" particle pusher[6] with the total electric field and a typical time step $\omega_{ce}\Delta t = 2\pi/32$. "Quiet-start" techniques[7] and k-space smoothing[8] are used in the computation to reduce the noise level. The modes retained are initially excited to approximately the same level but with random phases. The remaining parameters are different for the $\theta = 0$ and $\theta \neq 0$ cases, as follows:

<u>$\theta = 0$.</u> The system has 64 grid points and is 160 λ_{De} ($= v_e/\omega_{pe}$, initial electron Debye length) across; i.e., $\lambda_{De}/\Delta x = 0.4$. Usually 6400 electrons and 6400 ions are used. In one run we have doubled the number of particles and no appreciable difference in the results is observed.

<u>$\theta \neq 0$</u> . The system has 128 grid points and is 640 λ_{De} across ($\lambda_{De}/\Delta x = 0.2$). 14,000 electrons and 6,060 ions are used in the

simulations. The mass and charge of each ion cloud are proportionately increased so as to have charge neutrality in the system.

III. PHYSICAL SIMULATION PARAMETERS

Initially the plasma is distributed uniformly across the system. The particle initial velocity distributions as well as other parameters are different for the $\theta = 0$ and $\theta \neq 0$ cases.

$\underline{\theta = 0}$. Since $\vec{E}_{ext} \perp \vec{B}_o$ and $\vec{k} \perp \vec{B}_o$, there are no dynamics in the B_o direction. The electrons and ions have two dimensional Maxwellian velocity distributions, i.e., $f_{oj}(v_\perp) = (2\pi v_j^2)^{-1} \exp(-v_\perp^2/2v_j^2)$. Here $j = e,i$ and $v_\perp^2 = v_x^2 + v_y^2$. For equal electron and ion temperatures, we have $m_e v_e^2 = m_i v_i^2$. Thus, electron and ion initial random energy densities are $\bar{n}T_{o\perp} = \bar{n}m_e v_e^2$. Here $\bar{n}$ is the spatial-average particle density. The mass ratio used is $m_i/m_e = 50$. $\omega_{pi}/\omega_{ci} = 7$ and hence $\omega_{ce} \simeq \omega_{pe}$.

$\underline{\theta \neq 0}$. In this case the self-consistent electric field has a component along the $\vec{B}_o$ field. The electrons have a three-dimensional Maxwellian velocity distribution; $f_{oe}(v) = (2\pi v_e^2)^{-3/2} \cdot \exp(-v^2/2v_e^2)$. Since not only instabilities with both the (real) oscillation frequencies (ω_r) and growth rates (ω_i) much greater than ω_{ci} are expected but also the entire run is at least less than a half ion cyclotron period, we may treat the ions as unmagnetized to facilitate the computations. Since $\vec{k} \perp \vec{E}_{ext}$, the only ion dynamics are caused by the self-consistent electric field and ion motion perpendicular to $\hat{k}$ ($\hat{x}$) is ignored. Thus the ion velocity distribution is a one-dimensional Maxwellian in the $\hat{x}$-direction; i.e.,

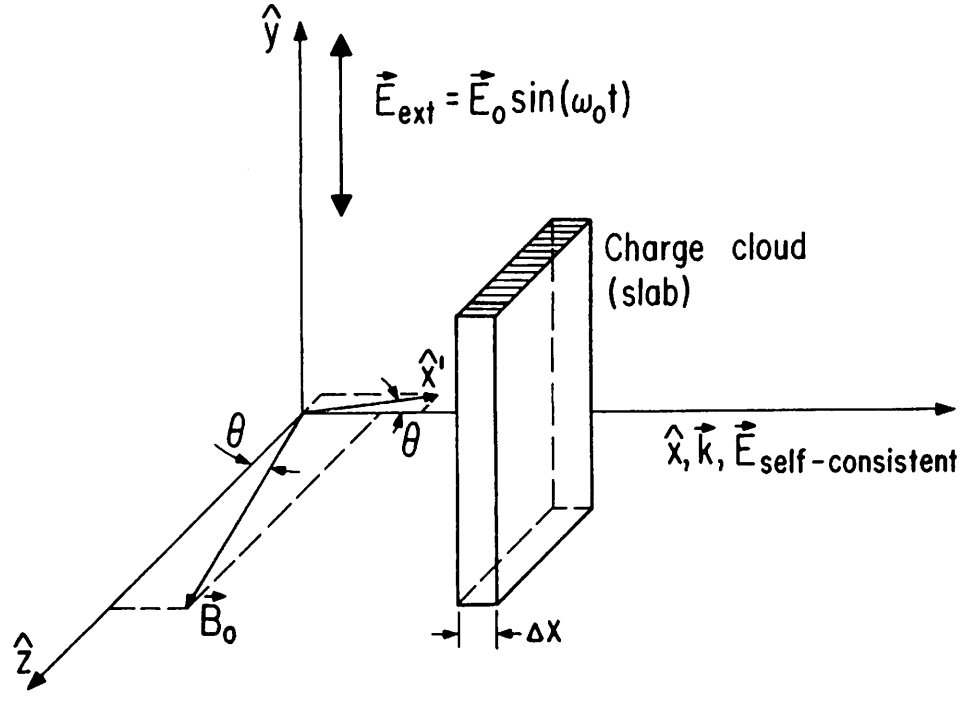

Fig. 1 The one-dimensional numerical simulation model. $\hat{x}$ is the direction of $\hat{y} \times \hat{B}_o$

TABLE 1. Summary of numerical and physical simulation parameters. $\pi/2 - \theta$ is the angle between the wave vector $\vec{k}$ and the magnetic field $\vec{B}_o$.

	$\theta = 0$	$\theta \neq 0$
$L/\Delta x$	64	128
$\lambda_{De}/\Delta x$	0.4	0.2
N_e	6400	14000
N_i	6400	6060
f_{oe}	2-D Maxwellian perpendicular to $\vec{B}_o$	3-D Maxwellian
f_{oi}	2-D Maxwellian perpendicular to $\vec{B}_o$	1-D Maxwellian in $\vec{k}$ (unmagnetized)
m_i/m_o	50	100
ω_{pi}/ω_{ci}	7	10
ω_{pe}/ω_{ce}	$\simeq 1$	1
$\omega_{ce}\Delta t = 2\pi/32$. Nominal cloud width = Δx.		
$E_{ext} = E_o \sin \omega_o t$. $\omega_o = \omega_{pi}$.		

$f_{oi}(v_x) = (2\pi v_i^2)^{-1/2} \exp(-v_x^2/2v_i^2)$. Initially we have $m_e v_e^2 = m_i v_i^2$. Thus, the initial electron random energy density in the perpendicular plane is $\bar{n}T_{o\perp} = \bar{n}m_e v_e^2$. Electron parallel and ion initial random energy densities are $\bar{n}T_{o\parallel} = \frac{1}{2}\bar{n}m_e v_e^2$. The mass ratio used in this case is $m_i/m_e = 100$. Furthermore, $\omega_{pi}/\omega_{ce} = 0.1$ and hence $\omega_{pe} = \omega_{ce}$.

At $t = 0$ the external electric field, $\vec{E}_{ext} = E_o \sin(\omega_o t)\,\hat{y}$, is applied uniformly across the system. Throughout our investigations, we have $\omega_o = \omega_{pi}$. The strength of E_o is indicated by the ratio of the drift speed to the electron thermal speed; $E_o/B_o v_e$.

Table 1 summarizes the numerical and physical simulation parameters described in the present and the preceding sections.

IV. REPRESENTATIVE SIMULATION RESULTS

Using the model described in the previous sections, we have investigated the dependence of plasma heating on θ and the parameter $E_o/B_o v_e$. For $\theta = 0$, we have $E_o/B_o v_e = 5, 7, 8.5$ and 10. A small θ is then introduced to see the effects of electron parallel (to $\vec{B}_o$) motion. For $\theta = (m_e/m_i)^{1/2} = 0.1$, we have $E_o/B_o v_e = 7$ and find the heating dynamics rather similar to those with $\theta = 0$. With a larger $\theta(\theta = 0.25)$, and $E_o/B_o v_e = 5$ and 7, the dynamics become entirely different from the previous ones. The results of three representative computer experiments are described in the following subsections.

(a) $\theta = 0$ and $E_o/B_o v_e = 8.5$. Fig. 2 shows the time evolution of the electrostatic field energy as well as the electron and ion spatial-average (perpendicular) kinetic energies relative to their respective spatial-average mean velocities, which we call (perpendicular) temperatures. (Note that this is a spatial-average temperature.) The field energy increases with several interesting features: (1) the over-all growth rate is exponential over about four orders of magnitude with average growth rate $0.4\omega_{pi}$; (2) the growth rate is first rapid then slow, with the larger rate occurring at the the peaks of the electron drift speed, and (3) there are high-frequency ($\sim 1.4\omega_{pe}$) structures. These observations clearly indicate the excitations of instabilities when the electron-ion relative streaming speed exceeds a certain threshold value. Further discussions on the instabilities will be given in the following Section.

At about $t = 12\ \bar{\tau}_{ce}$ (electron cyclotron period), when the field energy reaches an appreciable value $\varepsilon_w/\bar{n}\ T_{o\perp} \sim 0\ (10^{-1})$, both electron

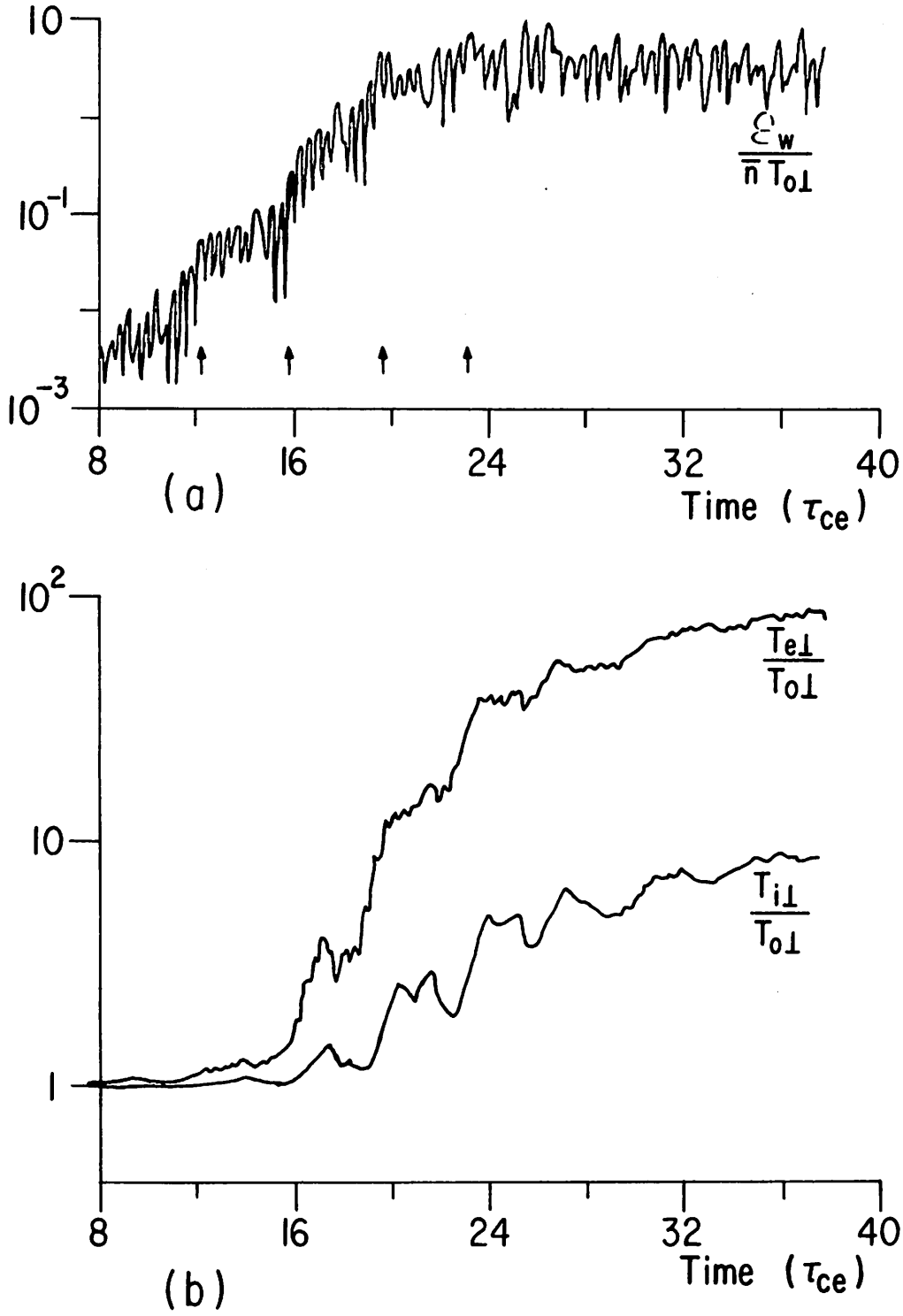

Fig. 2 Plots of (a) electrostatic field energy and (b) electron and ion perpendicular temperatures versus time in semi-logarithmic scales. The arrows indicate where the electron $\vec{E}_{ext} \times \vec{B}_o$ drift achieves its peak value E_o/B_o. τ_{ce} is the electron cyclotron period. Here $\theta = 0$ and $E_o/B_o\, v_e = 8.5$.

and ion (perpendicular) temperatures begin to increase rapidly. $T_{e\perp}$ increases with a rate faster than that of $T_{i\perp}$. ε_w saturates at $\varepsilon_{w,s}/\bar{n}T_{o\perp}\sim 10$ at about $t\simeq 26\tau_{ce}$; $T_{e\perp,s}/\bar{n}T_{o\perp}\sim 65$ and $T_{i\perp,s}/\bar{n}T_{o\perp}\sim 8$. At this time the rate of increase in temperature becomes much smaller. Before the saturation, temperatures are well correlated with the wave energy; that is, the rapid and slow increases occur together. After the saturation, ε_w stays more or less constant. Meanwhile, $T_{e\perp}$ and $T_{i\perp}$ increase at much slower rates, more or less linearly.

The growth rates and the time evolution of the wave spectrum of the first 15 significant spatial modes are shown in Fig. 3. The growth rates are measured for $t \simeq 12\ \tau_{ce}$ where the fields are small ($\varepsilon_w/\bar{n}T_{o\perp} \sim 10^{-2}$) so that these are considered to be the linear growth rates. The most unstable mode occurs at $k_m E_o/B_o = 1.65\ \omega_{im} = 0.45\ \omega_{pi}$. Before the saturation occurs, the wave spectrum is sharply peaked at the most unstable mode. In the post-saturation period the peak disappears and the spectrum decays with increasing wave number.

As shown by the phase-space (v_x vs. x) plots in Fig. 4, at $t \simeq 18\ \tau_{ce}$ (ε_w near saturation), the electrons are going rapidly into vortex-like motion due to trapping inside the wave potential troughs. (Earlier, the electron v_x - x space simply oscillates in v_x with no structure along x.) Around the saturation time both electrons and ions are well trapped. After the saturation, particles gradually smear out the ordered structures in the phase spaces and are, hence, thermalized. Throughout the run, electron (perpendicular) velocity distribution remains roughly isotropic.

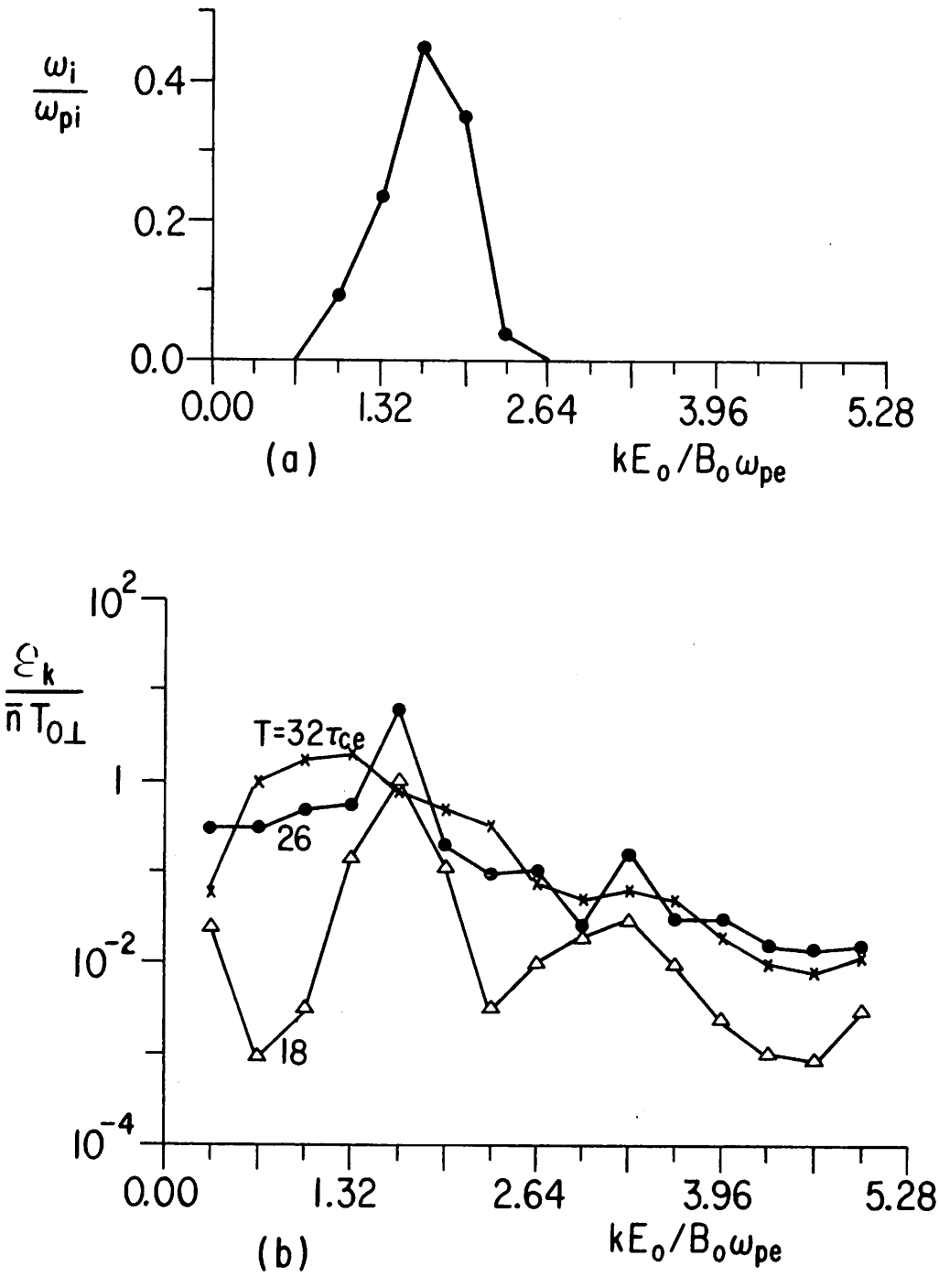

Fig. 3 Plots (a) measured linear growth rates and (b) wave spectrum at three different time steps vs. wave numbers. Here $\theta = 0$ and $E_o/B_o v_e = 8.5$.

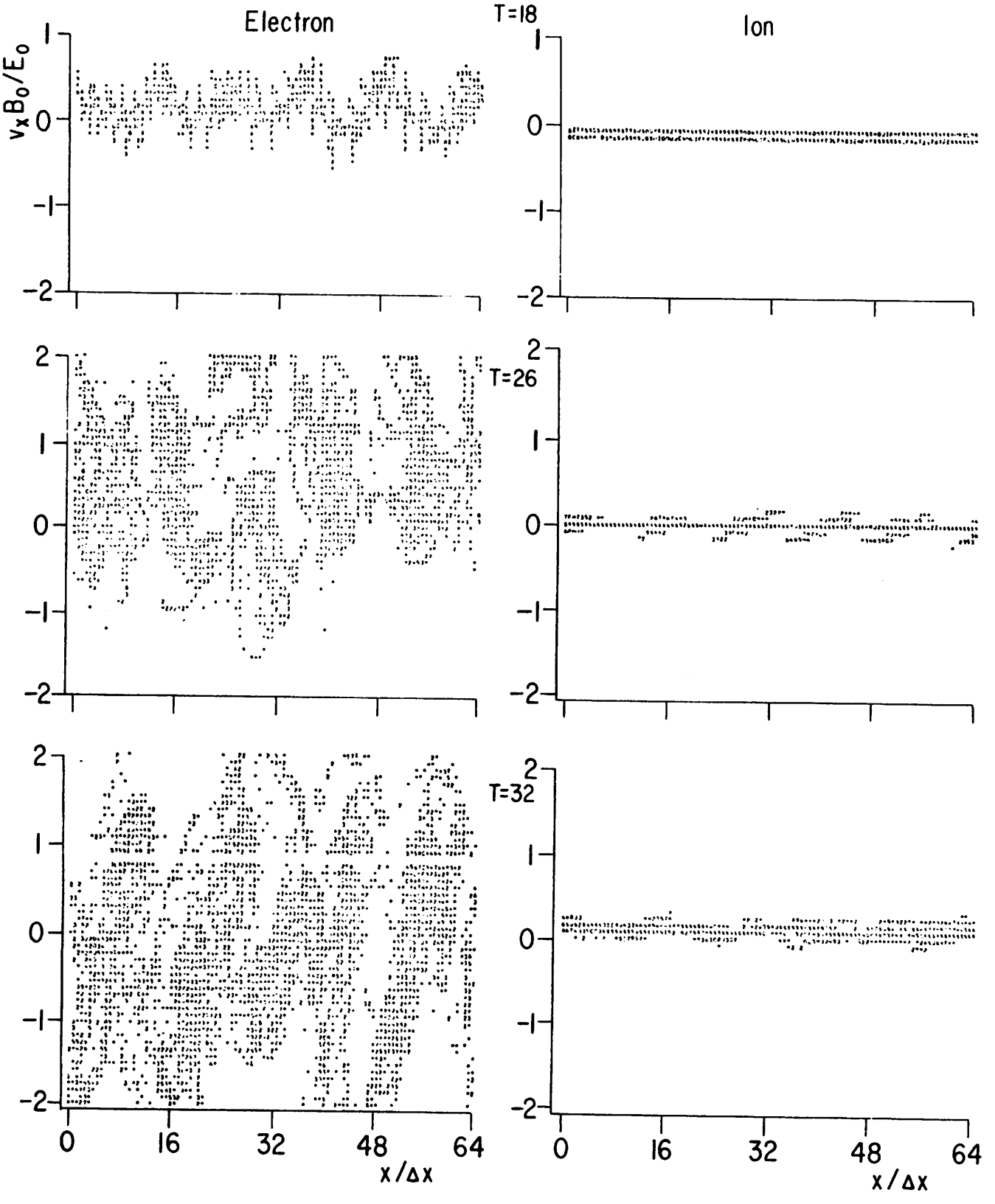

Fig. 4 Plots of the electron and ion phase spaces (v_x - x) at three different time steps. Here $\theta = 0$ and $E_o/B_o v_e = 8.5$. The horizontal blank near $v_x B_o/E_o = 1$ on the $T = 32\ \tau_{ce}$ electron plot is due to line-printer error.

(b) $\theta = 0.1$ and $E_o/B_o v_e = 7$. The time evolutions of field energy, electron perpendicular and parallel temperatures as well as ion temperature are shown in Fig. 5. Heating occurs mainly in the electron perpendicular temperature; $T_{e\perp,s}/T_{o\perp} \sim 43$. Ion heating is small, $T_{i,s}/T_{o\perp} \sim 10$. As to the electron parallel temperature, its heating rate is even smaller. Near the end of the run, $t = 40\tau_{ce}$, we find $T_{e\parallel}/T_{o\parallel} \sim 5.6$. The dynamics are rather similar to the previous $\theta = 0$ case. There, however, is a difference in the unstable modes. Fig.6 is a plot of the measured growth rates versus the wave numbers. While most of the unstable modes occur around $k_m E_o/B_o = 15.1\ \omega_{pi} = 1.51\ \omega_{pe}$ with $\omega_{i_m} = 0.37\ \omega_{pi}$, there is an additional unstable mode in the low-wave-number regime, $kE_o/B_o \simeq 0.7\ \omega_{pi}$ and $\omega_i \simeq 0.2\ \omega_{pi}$. As one increases θ and/or decreases $E_o/B_o v_e$, the low-wave-number modes become dominant; this is the next experiment.

(c) $\theta = 0.25$ and $E_o/B_o v_e = 5$. Fig. 7 shows the field energy as well as the various temperatures as functions of time. Contrasting to the previous two cases, the field energy exponentiated with a constant growth rate (no rapid then slow growth) $0.3\ \omega_{pi}$, indicating that the oscillating drifts exceed the instability threshold for a large fraction of the time. Also, the oscillating structure is of low frequency ($\sim 2\omega_{pi}$). As the wave energy grows, temperatures increase rapidly. Around $t = 32\ \tau_{ce}$ waves begin to saturate, $\varepsilon_{w,s}/\bar{n}\ T_{o\parallel} \sim 25$. About the same time the rate of heating decreases appreciably; $T_{e\parallel,s}/T_{o\parallel} \sim 140$, $T_{e\perp,s}/T_{o\perp} \sim 30$ and $T_{i,s}/T_{o\parallel} \sim 75$.

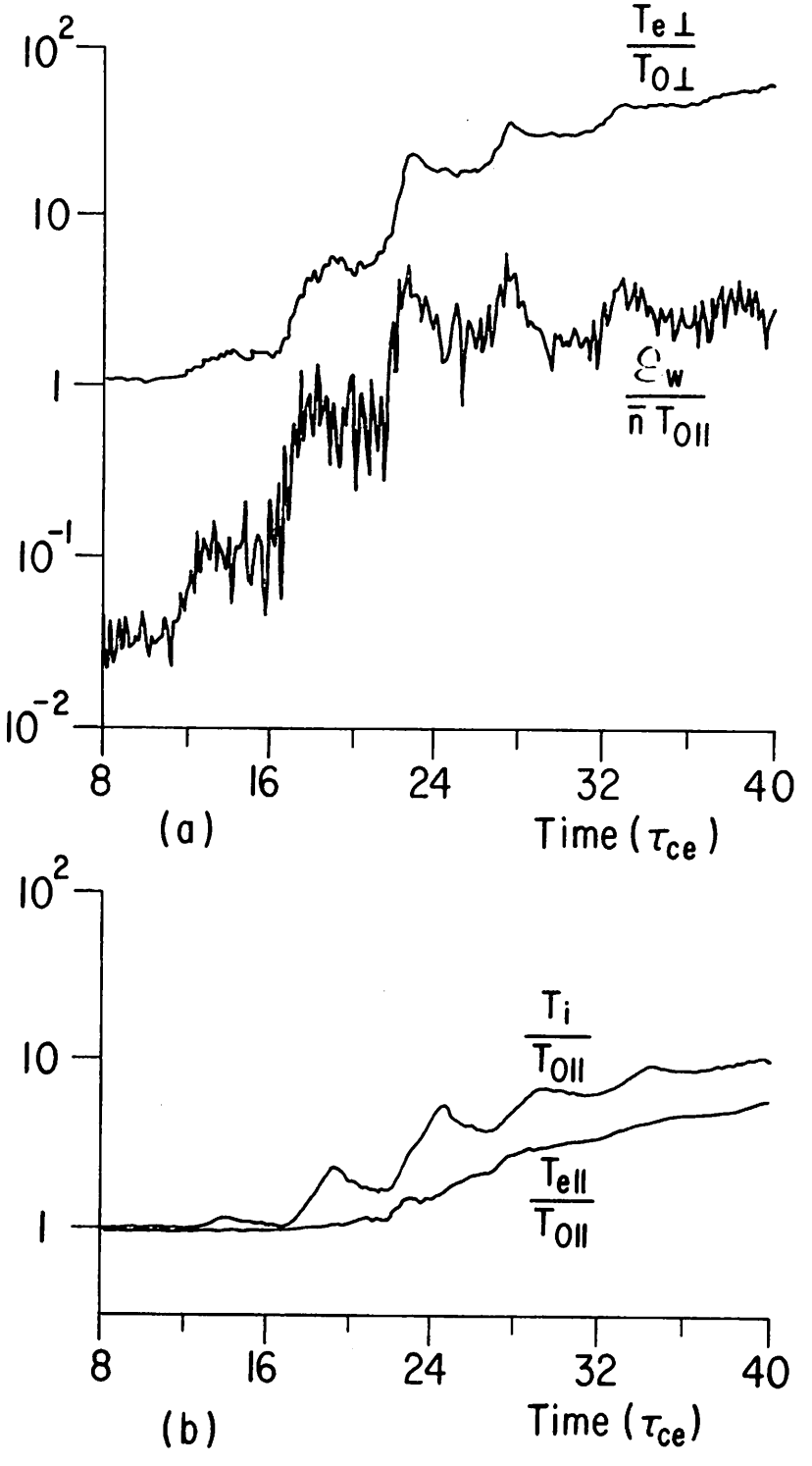

Fig. 5 Plots of (a) electrostatic field energy as well as electron perpendicular temperature and (b) electron parallel and ion temperatures vs. time in semi-logarithmic scales.
Here $\theta = (m_e/m_i)^{1/2} = 0.1$ and $E_o/B_o v_e = 7$.

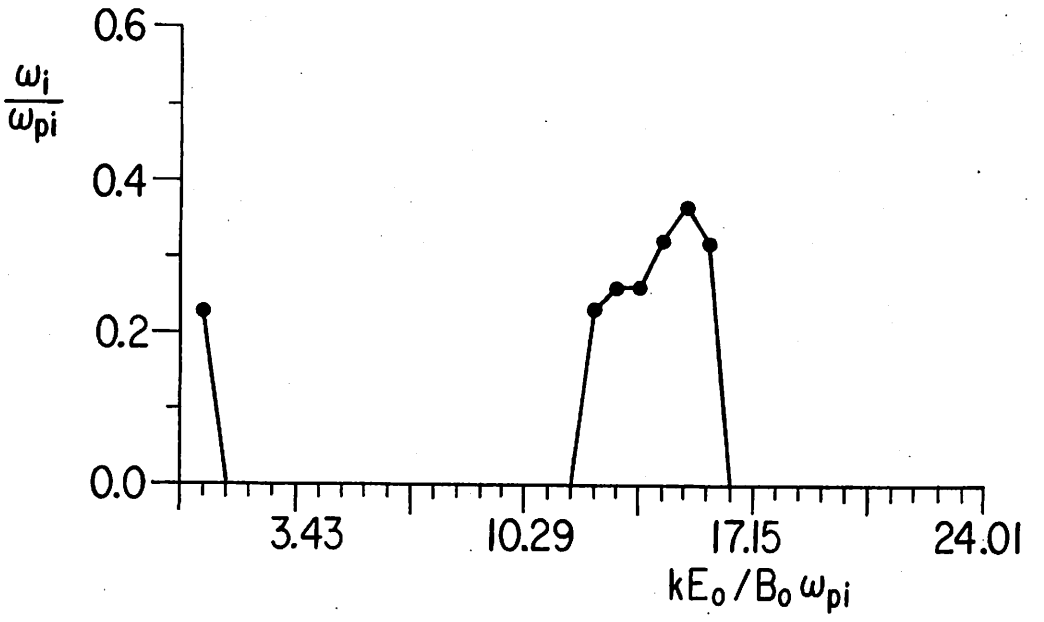

Fig. 6 Plot of the measured linear growth rates vs. wave numbers Here $\theta = 0.1$ and $E_o/B_o v_e = 7$.

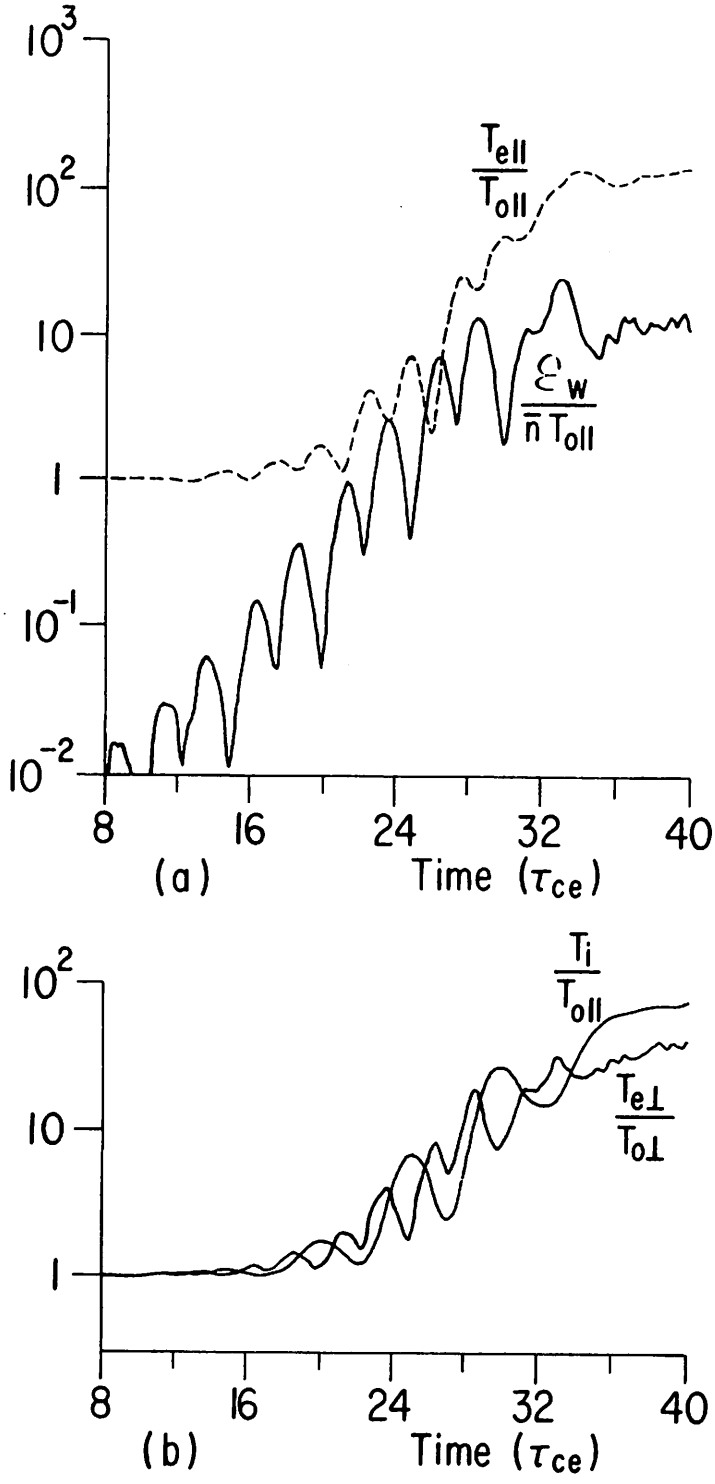

Fig. 7 Plots of (a) electrostatic field energy and electron parallel temperature and (b) electron perpendicular and ion temperatures vs. time in semi-logarithmic scale. Here $\theta = 2.5\,(m_e/m_i)^{1/2} = 0.25$ and $E_o/B_o v_e = 5$.

Thus, electrons are mainly heated up in the parallel direction and there is also considerable ion heating. After the saturation wave energy stays more or less constant while temperatures slowly increase.

The measured growth rates and the wave spectrum of the first significant 32 modes are shown in Fig. 8. Dominant unstable modes have relatively small wave numbers with $k_m E_o/B_o = 2.45\ \omega_{pi}$ and $\omega_{im}=0.37\ _{pi}$. There are also unstable modes at larger wave numbers; $kE_o/B_o \simeq 1.47\omega_{pe}$ and $\omega_i \simeq 0.1\omega_{pi}$. Before the saturation the spectrum is sharply peaked around the fastest growing mode. As the waves saturate the peak disappears and the spectrum decays with increasing wave number.

Various phase-space plots of electrons and ions are illustrated in Fig. 9. v_x, is the velocity component in the $\hat{y} \times \vec{B}_o$ direction (referring to Fig. 1). Around the saturation both electrons and ions are well trapped. Electron trapping and heating are mainly along $\vec{B}_o$. Before the saturation, the dominant perpendicular electron dynamics are in the $\hat{y}$ direction rather than in $\hat{x}'$. As the waves saturate, particles begin to smear out the phase space and are gradually thermalized. Meanwhile, electron perpendicular velocity distribution becomes more isotropic.

We now summarize the contrasts among the above three representative computer experiments:

(a) $\theta = 0$ and $E_o/B_o v_e = 8.5$. (Parallel motion is ignored.)
The instability has rapid-slow growth, with rapid growth occurring when the speed of electron-ion relative drift is near its peak

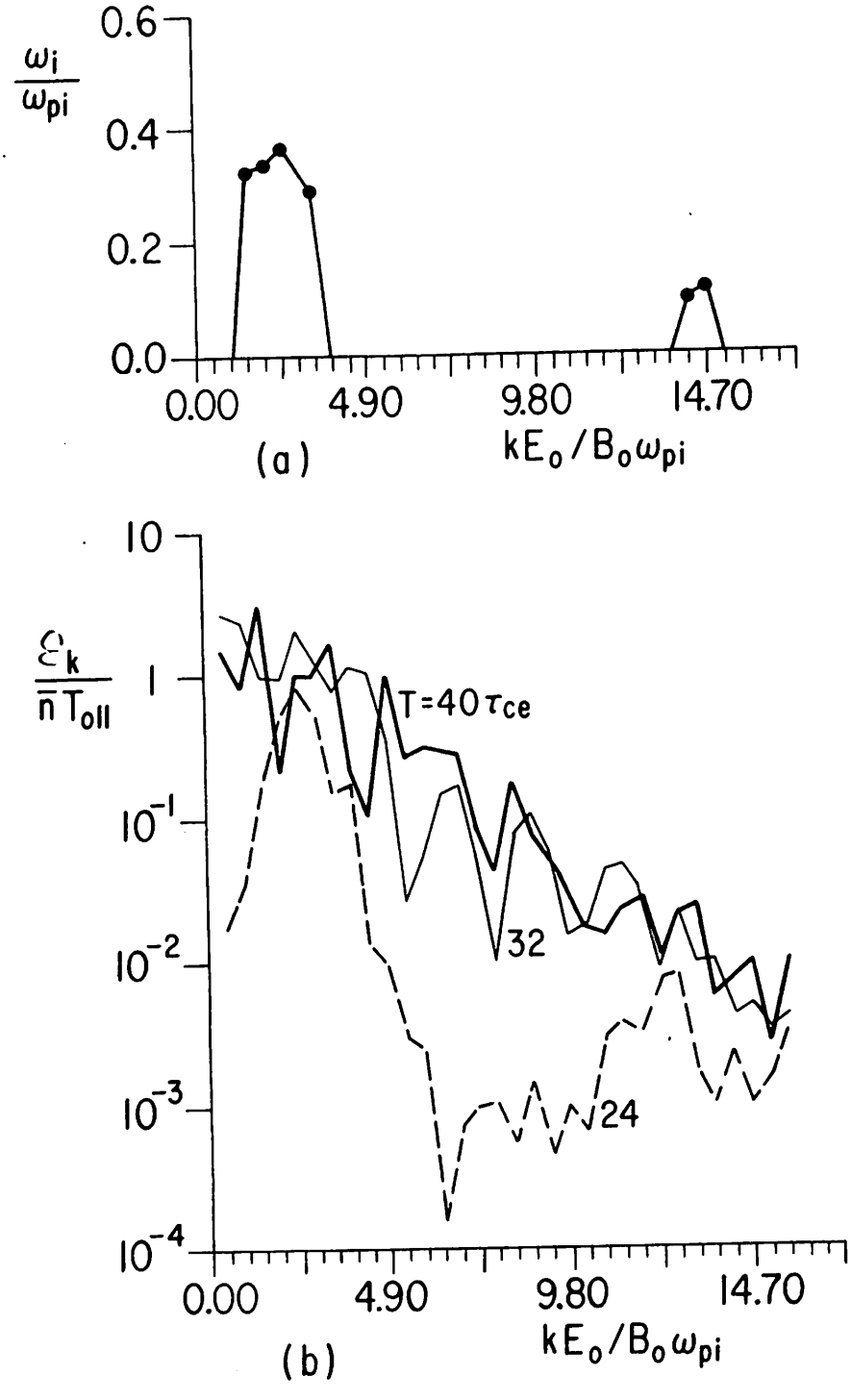

Fig. 8 Plots of (a) the measured linear growth rates and (b) the wave spectrum at three different time steps vs. wave number. Here $\theta = 0.25$ and $E_o/B_o v_e = 5$.

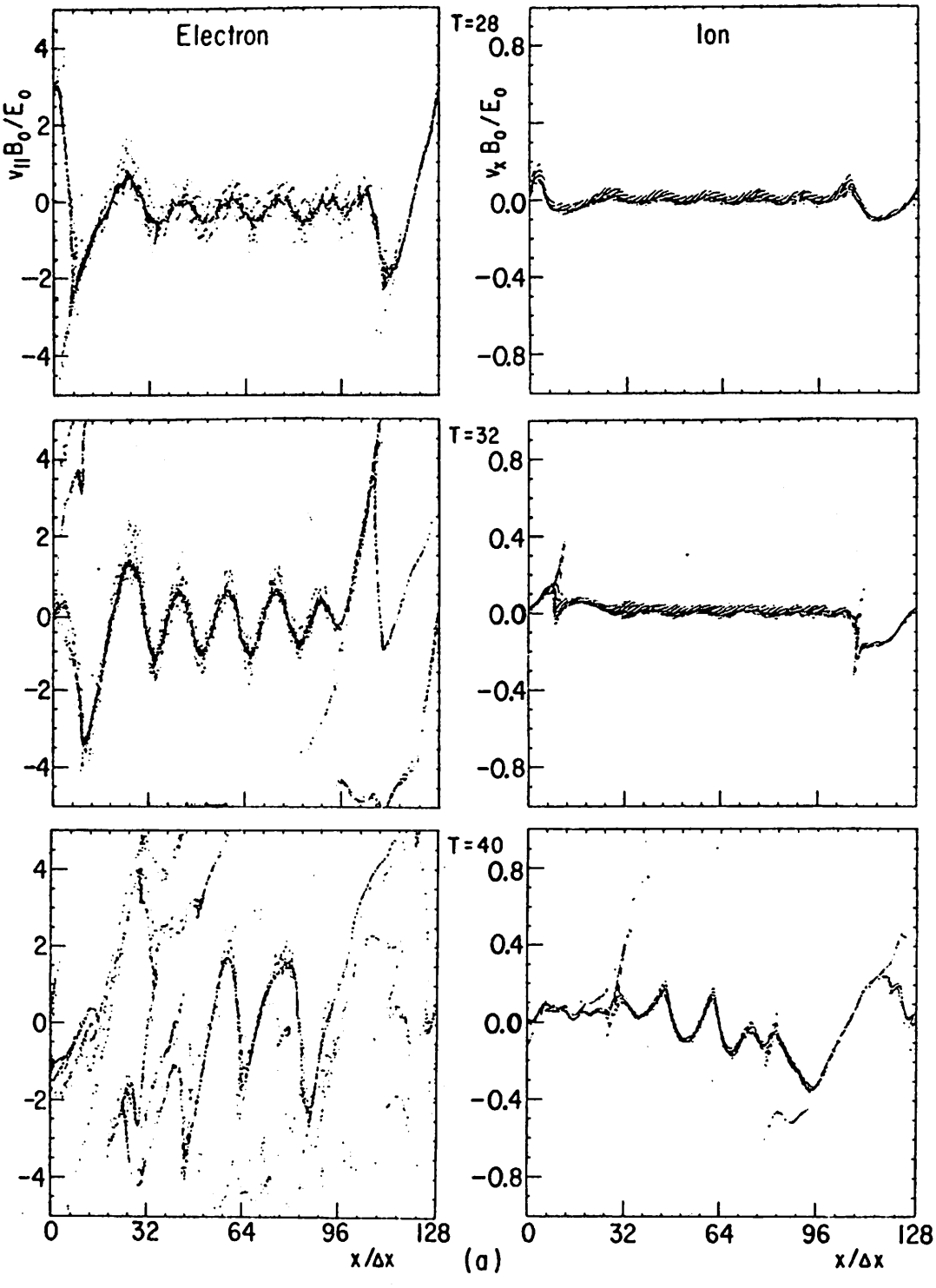

Fig. 9 Plots of various phase spaces at three different time steps. (a) electron ($v_{\parallel}$ - x) and ion (v_x - x). (b) electron (v_x - x) and (v_y - x). Here $\theta = 0.25$ and $E_o/B_o v_e = 5$.

value, E_o/B_o. Unstable modes occur near $k_m E_o/B_o = 1.65\ \omega_{pe}$. There is strong heating in the electron (perpendicular) temperature. Ion (perpendicular) heating is small. Electron (perpendicular) velocity distribution remains approximately isotropic.

(b) $\theta = 0.1$ and $E_o/B_o v_e = 7$. (Ions are unmagnetized.) The results are similar to those of experiment (a) except there is an additional low-wave-number ($kE_o/B_o \simeq 0.7\ \omega_{pi}$) unstable mode. Electron parallel heating is rather small.

(c) $\theta = 0.25$ and $E_o/B_o v_e = 5$. (Ions are unmagnetized.) The instability has a uniformly exponential growth. The dominant unstable mode occurs at small k; $k_m E_o/B_o = 2.45\ \omega_{pi}$. There are also unstable modes at larger k; $k\ E_o/B_o \simeq 1.47\ \omega_{pe}$. Strong heatings occur in electron parallel and ion temperatures. Before the waves saturate, electron dynamics in the perpendicular direction are mainly in the $\hat{y}(\vec{k} \times \vec{B}_o)$ direction.

These results, thus, suggest the following pictures: (1) instabilities are excited by the electron E/B drift through the ions; (2) for small $\theta(\lesssim\sqrt{m_e/m_i}\,)$, the dominant instability is at larger k and has a threshold in the drift speed near v_e; (3) increasing θ shifts the dominant instability to smaller k with a much smaller instability threshold; (4) as the wave energy becomes large , particles execute vortex-like motion in the phase space (i.e., they are trapped by the waves) and rapid heatings occur; (5) the dynamics of particle trapping and, hence, heatings are different for the two types of instabilities described in (2) and (3).

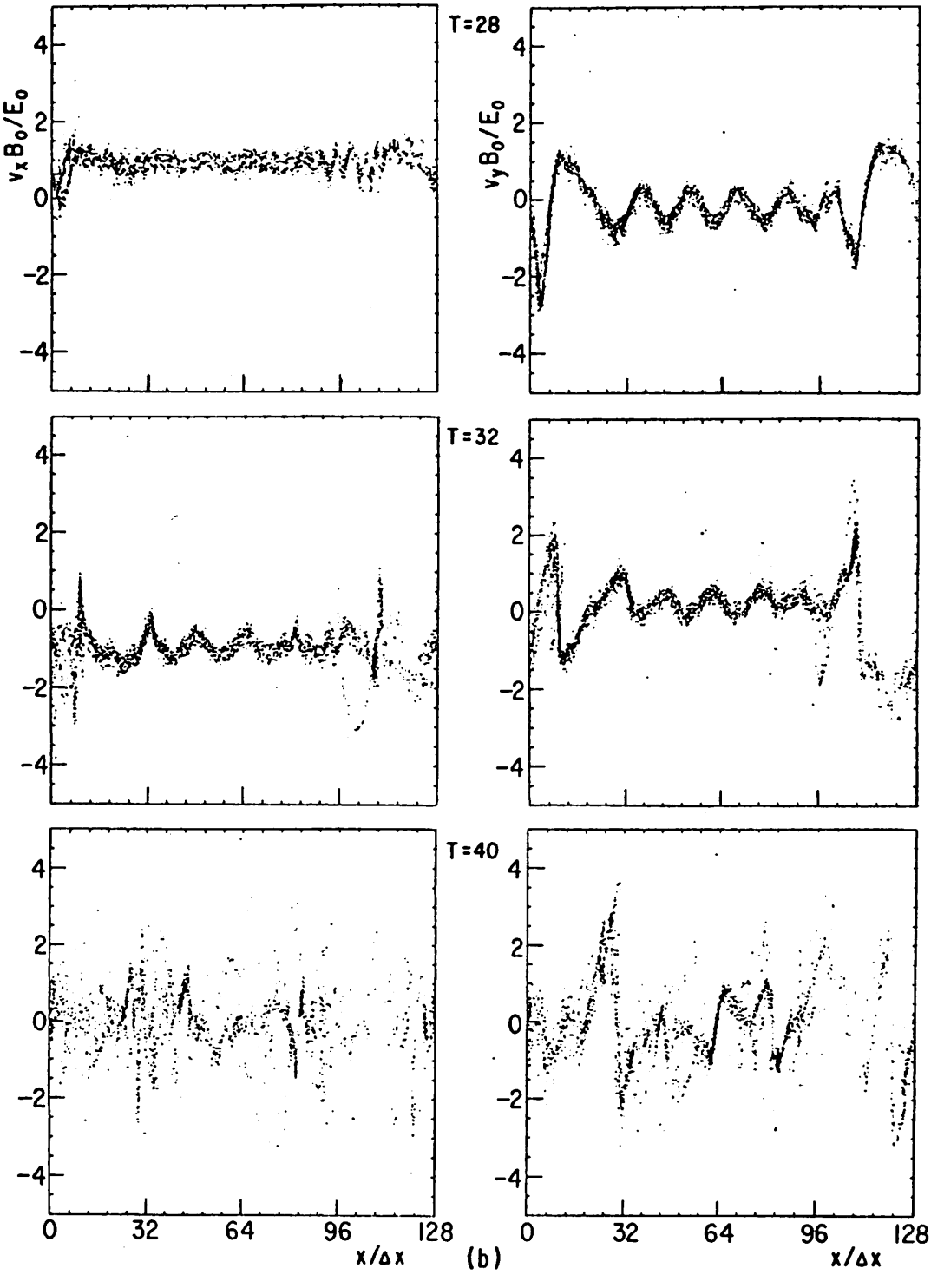

Fig. 9 (continued)

V. THEORIES AND COMPARISONS WITH SIMULATION RESULTS

In this section we seek to understand the simulation results on a theoretical basis. First, linear instabilities due to a steady electron-ion relative drift are analyzed. Then we examine the non-linear evolutions of the instabilities and estimate the relevant physical quantities. In each stage, simulation results are compared with the corresponding theoretical predictions and estimates.

A. Linear Instability. The theoretical model considered here is sketched in Fig. 10. The plasma is Maxwellian with $T_e \sim T_i$. It is the same as the simulation model except that (1) for convenience we choose here to work in the electron frame (electrons not drifting) and (2) instead of having $\vec{E}_{ext}$ to provide the drift, we assume that the ions have a steady drift $\vec{U}$ in the $\hat{x}'$ direction (that of $\vec{U} = \vec{E}_{ext} \times \vec{B}_o$). Here U is assumed to be much greater than v_e. Electrostatic waves with $|\omega - \vec{k}\cdot\vec{U}|^2 >> \omega_{ci}^2$ are considered; therefore ions are treated as unmagnetized. This model (or similar ones) has long been the attention of theoretical studies on drift-excited electrostatic instabilities in magnetized plasmas.[9-13] Here we redo some parts of the theory so that the results are more applicable for comparisons with the simulation results. Specifically, we look for (1) hydrodynamic non-resonant instabilities and (2) how the properties of the instabilities change as θ changes. Assuming $kv_e/\omega_{ce} < 1$, $|\omega - \vec{k}\cdot\vec{U}| > kv_i$ and $|\omega| > k_{\parallel} v_e$; i.e., ignoring resonant particles effects, we can treat the plasma in the fluid limit. (These assumptions are justified by the results obtained later.) The dispersion relation then is

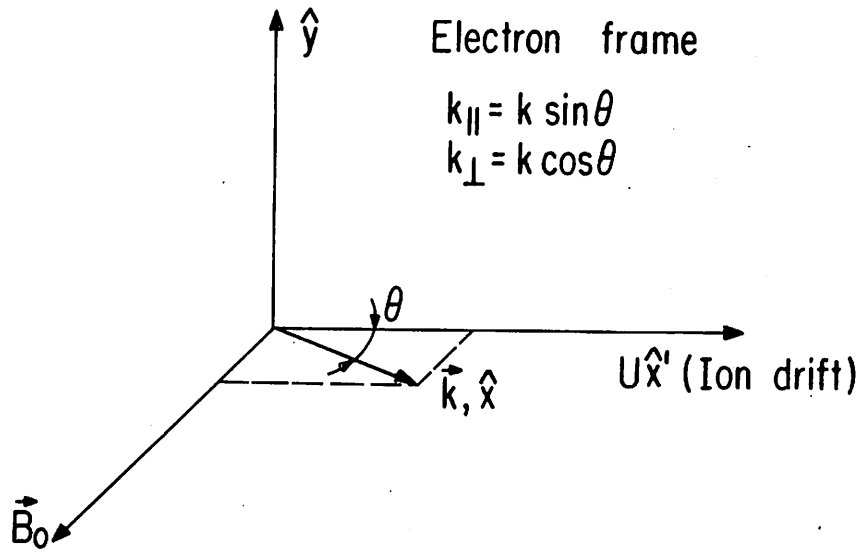

Fig. 10 Theoretical model for drift-excited instabilities. Electrons have no drift; $T_e \sim T_i$.

$$1 - \cos^2\theta \frac{\omega_{pe}^2}{\omega^2 - \omega_{ce}^2} - \sin^2\theta \frac{\omega_{pe}^2}{\omega^2} - \frac{\omega_{pi}^2}{(\omega - k\ U\cos\theta)^2} \quad 0. \quad (1)$$

This dispersion relation was first investigated by Buneman.[9] The term $\cos^2\theta \frac{\omega_{pe}^2}{\omega^2 - \omega_{ce}^2}$ is due to the electron polarization drift across the magnetic field, while $\sin^2\theta \frac{\omega_{pe}^2}{\omega^2}$ comes from electron motion along the magnetic field. Corresponding to our simulation parameters; $m_e/m_i = 0.01$, $\omega_{pe}/\omega_{ce} = 1$, $\omega_{pe} = 10\ \omega_{pi}$ and three different values of θ, (1) is solved numerically. The unstable roots are shown in Fig. 11.

The existence of high-frequency ($\omega_r \geq \omega_{ce}$) instability (hereafter called upper-hybrid two-stream instability) was predicted by Buneman.[9] The frequency and growth rate of the most unstable mode for $\theta << 1$ are

$$k_m U\cos\theta \sim k_m U = \omega_{UH} = (\omega_{pe}^2 + \omega_{ce}^2)^{1/2} ,$$

$$\omega_{im} = 0.69\ \omega_{pi}\ (m_i/m_e)^{1/6}\ (\omega_{pe}/\omega_{UH})^{1/3} \quad (2)$$

and $$\omega_{rm} = \omega_{UH} - 0.4\ \omega_{pi}\ (m_i/m_e)^{1/6}\ (\omega_{pe}/\omega_{UH})^{1/3} .$$

These predictions agree with the numerical solutions. With $\omega_{ce} \geq \omega_{pe}$, $\theta << 1$ and $\omega^2 \geq \omega_{ce}^2$ we have

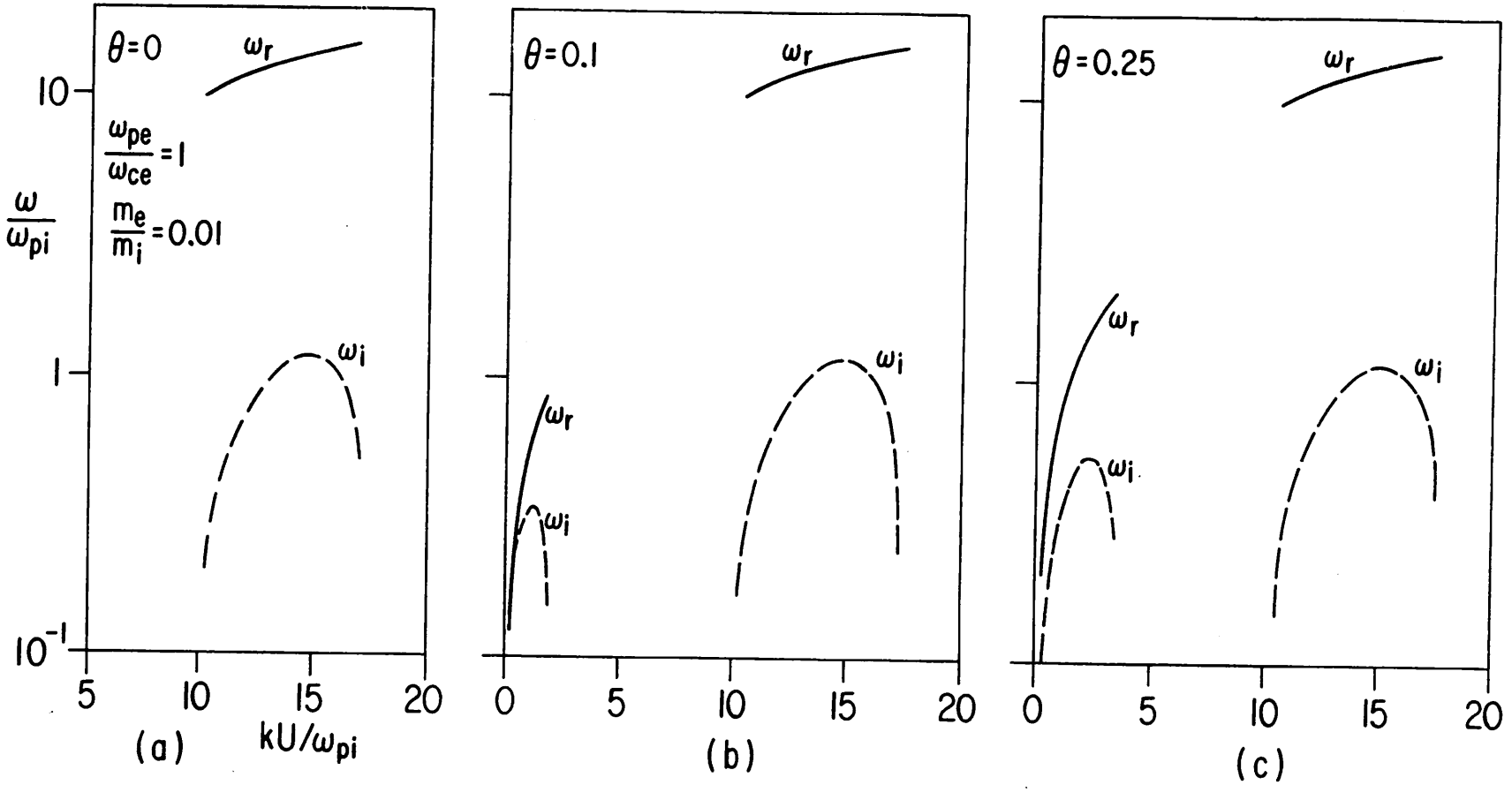

Fig. 11 Plots of unstable roots for $\theta = 0$, $(m_e/m_i)^{1/2}$ and $2.5\,(m_e/m_i)^{1/2}$. Here $m_e/m_i = 0.01$ and $\omega_{pe}/\omega_{ce} = 1$. The scales are semi-logarithmic.

$$\sin^2\theta\,\frac{\omega_{pe}^2}{\omega^2}\sim\theta^2\,\frac{\omega_{pe}^2}{\omega_c^2}\;\ll\;\cos^2\theta\,\frac{\omega_{pe}^2}{\omega^2-\omega_{ce}^2}\sim\;\frac{\omega_{pe}^2}{\omega^2-\omega_{ce}^2}\quad .$$

(Parallel motion term) << (Perpendicular motion term).

Thus at least during the initial stage of the instability electron motion is expected to be mainly in the perpendicular plane. Dropping the parallel term, (1) approximates as

$$1-\frac{\omega_{pe}^2}{\omega^2-\omega_{ce}^2}-\frac{\omega_{pi}^2}{(\omega-kU)^2}\simeq 0\quad . \tag{3}$$

Hence, for this instability there is little difference in dynamics between $\theta = 0$ and $\theta \ll 1$.

As θ becomes non-zero, a new branch of the instability begins to emerge at low frequency ($\omega_r \sim \omega_{pi}$) and low wave number ($kU \sim \omega_{pi}$). This instability was predicted by Krall and Liewer[13] and has been called a modified two-stream instability. For $\theta \sim (m_e/m_i)^{1/2} \ll 1$, the frequency and growth rate of the fastest growing mode are given by

$$\omega_{rm}\sim\omega_{im}\;\sim\;\omega_{pi}\,\frac{\omega_{ce}}{\omega_{UH}} \tag{4}$$

and $$k_m U \sim \omega_{rm}$$

Our numerical solutions agree with the above results. An attractive feature of this instability is its low threshold for drift speed,

as follows. Unlike upper-hybrid two-stream instability which requires $U > v_e$, modified two-stream instability only requires $U > \left[(T_e + T_i)/m_i\right]^{1/2} \sim v_i$ for $T_e \sim T_i$[13]. With $\theta^2 << 1$ and $\omega^2 \sim \omega_{pi}^2$, (1) is approximated as

$$\frac{\omega_{UH}^2}{\omega_{ce}^2} - \theta^2 \frac{\omega_{pe}^2}{\omega^2} - \frac{\omega_{pi}^2}{(\omega - kU)^2} \simeq 0 \quad . \tag{5}$$

Hence electrons are free to accelerate only along the magnetic field and, as recently pointed out by Ott et al.,[14] electrons behave as if they had an effective mass $\bar{m}_e = m_e k^2/k_{\parallel}^2 = m_e\theta^{-2}$. Meanwhile, electron perpendicular motion is mainly E/B drift induced by the wave electric field. Due to the effective increase in electron mass, one then expects stronger ion responses. All the above properties have been observed in the simulation works of Ott and others.

As borne out by Fig. 11, ω_{im} and the spectrum width in k of the modified two-stream instability increase with θ, while those properties of the upper-hybrid two-stream instability undergo little change. Modified two-stream instability thus becomes more dominant as θ increases. However, in order to avoid electron Landau damping ($\omega_r > v_e k \sin\theta$), it is necessary to have $\theta \lesssim \theta_m \sim \tan^{-1}(U/v_e)$. For $U/v_e \geq 1$, this condition can be satisfied for a wide range of θ.

Based on the above discussions, we can begin to understand the linear instabilities observed in simulations. For $\theta = 0$ the instability excited is the upper-hybrid two-stream instability with theoretically $k_m U \simeq \omega_{UH}$ and ω_{UH} and $\omega_{im} \simeq 1.2\ \omega_{pi}$. For a sinusoidally oscillating electron drift (as in the simulations), $U(t) \simeq \frac{E_o}{B_o} \sin \omega_o t$, one then expects that this instability will be excited during the fraction of the cycle when the drift speed exceeds the instability threshold value (see Fig. 12). Since $\frac{dU(t)}{dt} = 0$ at $|U(t)| = E_o/B_o$, therefore $|U(t)| \simeq E_o/B_o$ for the longest period during each oscillating cycle. Thus, only the waves with waves numbers $|k| \simeq \omega_{UH} B_o/E_o$ will have the longest growing time during each cycle and, hence, will be the dominant mode, i.e., $k_m E_o/B_o \simeq \omega_{UH}$ is expected. Furthermore, the instability will grow in a stepwise fashion as observed in the simulations. Since the two oppositely-propagating waves with $k = \pm\omega_{UH} B_o/E_o$ will grow only during each half cycle, the growth rate is expected to be $\omega_{im} \simeq 0.5\ (\frac{\pi-2\theta_o}{\pi})\ 1.2\ \omega_{pi} + 0.05\omega_o$. Here $\theta_o = \sin^{-1}(v_{thresh}/U)$, and in our case we have $\theta_o \sim v_e/U << 1$ and $\omega_{im} \simeq 0.65\omega_{pi}$. Fig. 13 is a plot of $k_m E_o/B_o$ and ω_{im} vs. $E_o/B_o v_e$, respectively. The average measured value of $k_m E_o/B_o$ is $1.6\ \omega_{pe}$. The discrepancy with the theoretical value, $1.4\ \omega_{pe}$, may be due to the discreteness of the wave numbers. For $E_o/B_o v_e \gtrsim 8$, ω_{im} approaches a constant value, $0.45\ \omega_{pi}$; which is close to the estimated value, $0.65\omega_{pi}$. As $E_o/B_o v_e$ decreases below 8, ω_{im} decreases, more or less linearly toward zero. That waves propagating in opposite directions are excited may create certain standing waves and,

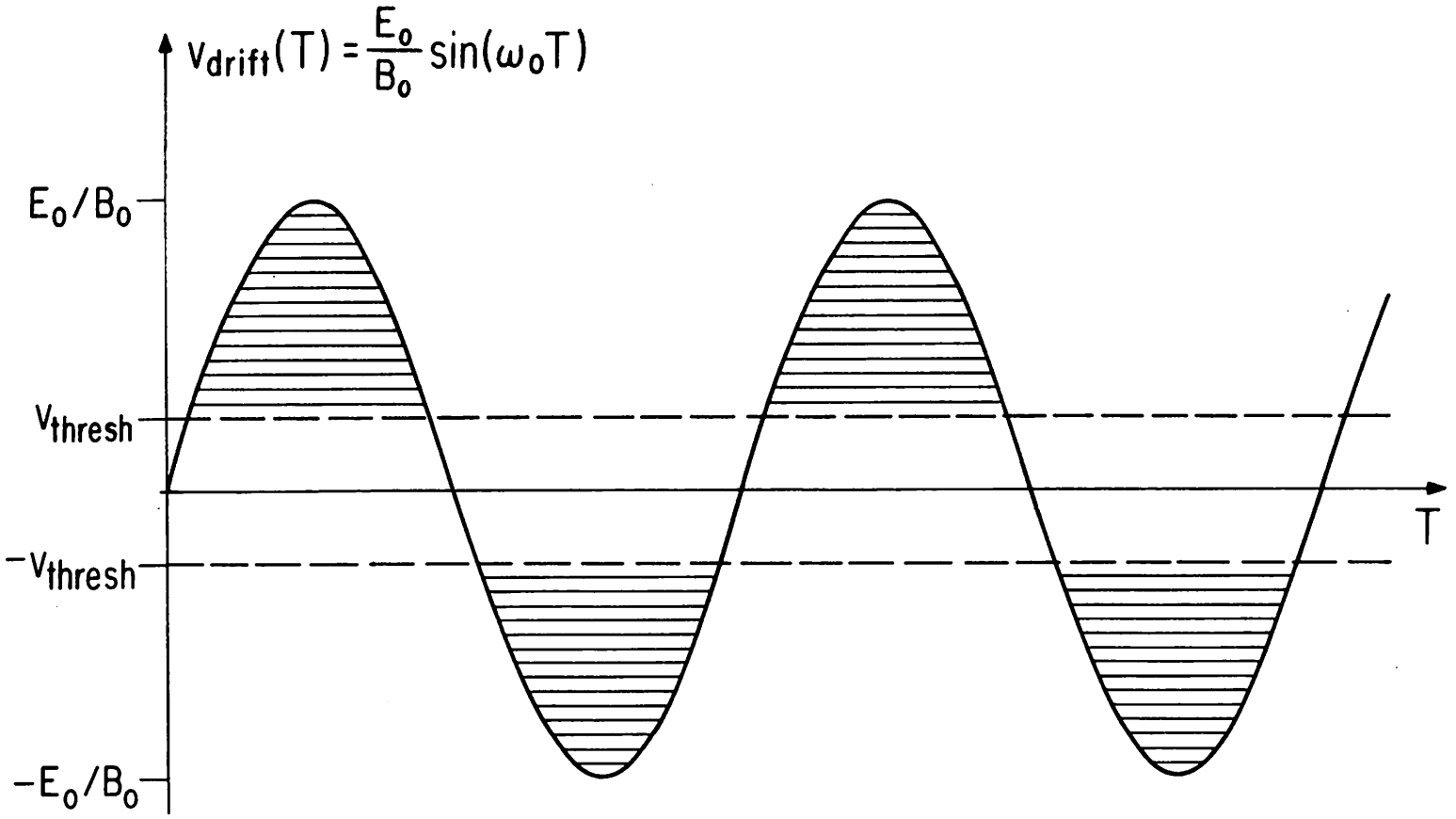

Fig. 12 A sketch of the model of instability mechanism. Instability is excited when $V_{drift} > v_{threshold}$ (shaded region). For upper-hybrid-two-stream instability, $v_{thresh} \sim v_e$. For modified two-stream instability, $v_{thresh} \sim v_i$.

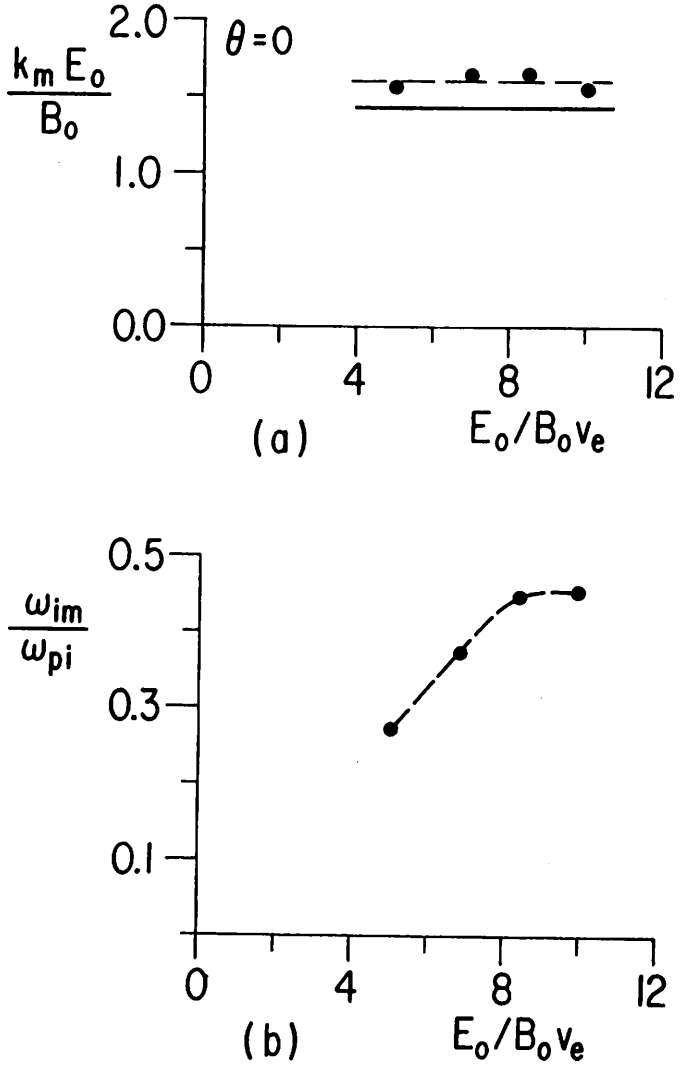

Fig. 13 Plots of measured (a) $k_m E_o/B_o$ and (b) ω_{im}/ω_{pi} vs. $E_o/B_o v_e$. Here $\theta = 0$. The solid line indicates the theoretically estimated value.

therefore, explains the oscillating structures seen in the simulations.

For non-zero θ, the emergence of low-wave-number instability in the simulations is due to the presence of modified two-stream instability. For small θ, e.g., in experiment (b), this instability has relatively small growth rate and narrow spectrum and, therefore, the dominant instability is still the upper-hybrid two-stream instability. As one increases θ and reduces $E_o/B_o v_e$ (i.e., the growth rate of the upper-hybrid two-stream instability), modified two-stream instability will take over and become the dominant instability. This is what we have observed in experiment (c). The measured value of $k_m E_o/B_o$ is 2.45 ω_{pi}, while the estimated value is 2.25 ω_{pi}. The agreement is rather good. Furthermore, due to its low threshold $\sim v_i$ (Fig. 12), this instability has a constant growth rate and the observed maximum growth rate is 0.37 ω_{pi} which is close to the estimated value, $0.5 \times 0.54\omega_{pi} + 0.05\omega_{pi} = 0.32\omega_{pi}$.

B. Nonlinear Evolutions. As suggested by the simulation results, the nonlinear evolution of the excited instability is strongly associated with particle trappings by the observed rapid heatings as well as the saturation of the instability. For each instability, the trapping dynamics and heating are different. Using trapping arguments, we therefore have constructed nonlinear theories for the two types of instability mentioned above.

1. Upper-hybrid two-stream instability. Since, as suggested both from the simulations results and the linear dispersion relation, this instability interacts with electrons mainly in the perpendicular direction, we take the wave vector, $\vec{k}$, to be perpendicular to $\vec{B}_o$ and ignore electron motion along $\vec{B}_o$. The approach used here is similar to that of Forslund et al.,[15] except here we have $kr_e = kv_e/\omega_{ce} << 1$ (i.e., the instability is non-resonant).

A sketch of wave and particle force potentials in the electron frame shown in Fig. 14, for use in modelling electron trapping. The model is not wholly self-consistent. Let us consider those electrons which have guiding centers at $x = 0$ and temperature $T_e = m_e v_e^2$. The electrostatic wave, $\phi(x,t) = \phi_o \cos(kx-\omega t)$, propagates in the x-direction. Here ϕ_o is assumed to be a constant. Since the spectrum is sharply peaked at the fastest growing mode, we take $\omega = \omega_{rm} \simeq \omega_{UH}$ and $k = k_m = \omega_{UH}/U$. Thus the wave phase velocity is $\omega/k \simeq U >> v_e$. The motion of electrons then can be determined from the combined potential, $\bar{\phi} = -e\phi + m_e\omega_{ce}^2 x^2/2$, due to the wave potential and the magnetic field. Away from $x = 0$, the relative effect of the wave potential becomes weaker due to the increasing $\vec{v} \times \vec{B}_o$ force and, eventually, the combined potential troughs vanish at $|x| = x_v \simeq ek\phi_o/m_e\omega_{ce}^2$ (v here stands for vanish) where, physically, the wave electric force equals the magnetic force due to B_o.

Since $kr_e << 1$ electrons sample only a small portion of a single potential trough. The time during which an electron sees a single trough is $\tau \sim \lambda/2U \sim \pi/\omega \sim \pi/\omega_{UH}$. In the absence of $\vec{B}_o$, an electron will be trapped if during this time period τ it can execute several

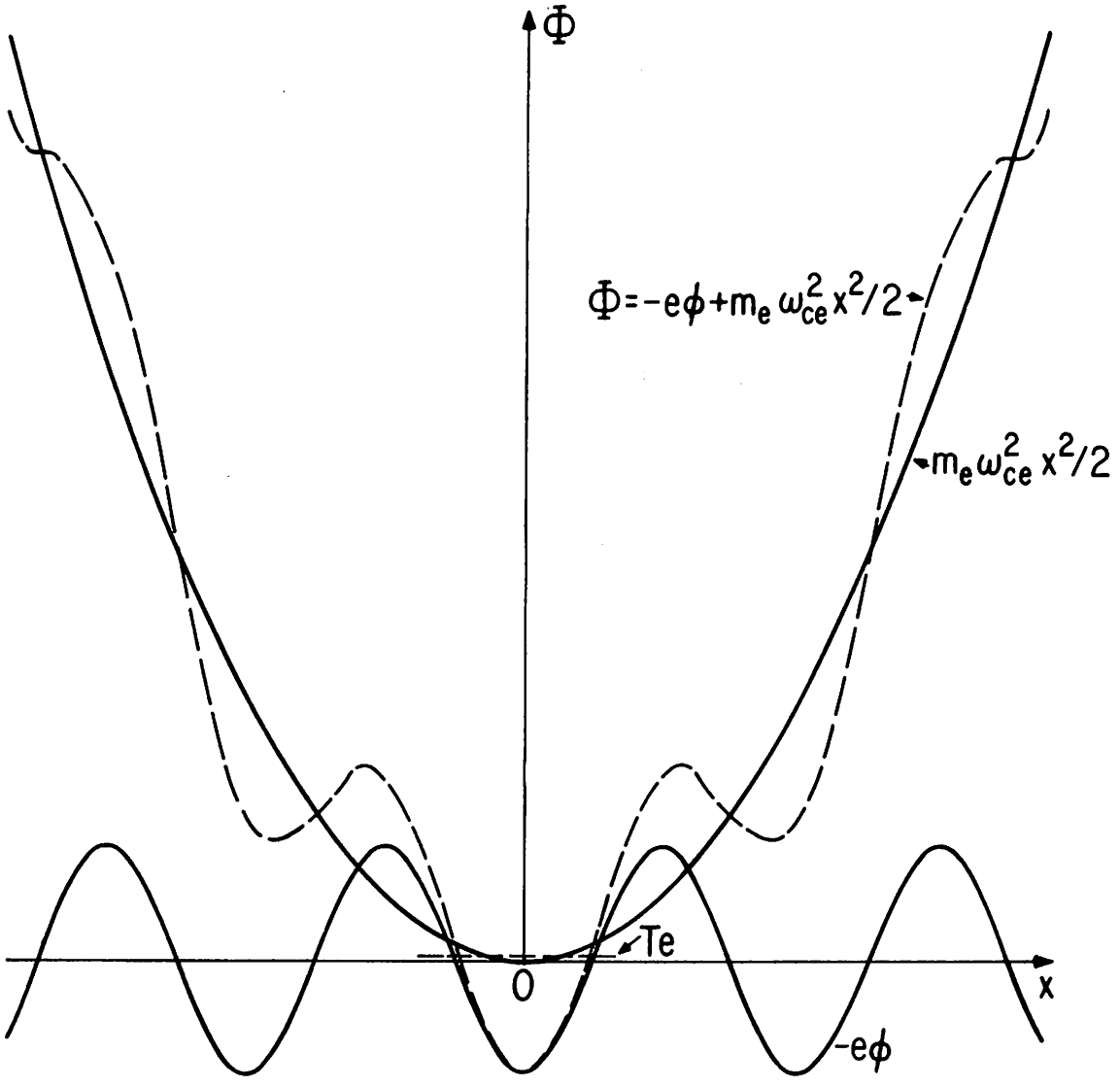

Fig. 14 The non-self-consistent model of electron trapping by a longitudinal electrostatic wave propagating perpendicularly to $\vec{B}_o$. The model is in the electron frame. T_e is the electron random kinetic energy before the electrostatic wave is imposed; thus, the intersection between T_e and the magnetic well indicates the Larmour radius. That the wave through is in phase with the magnetic well is for the convenience of illustrating the concepts.

bounce oscillations inside the trough. With the magnetic field present, however, a trapped electron can only stay in the travelling trough for a period x_v/U before it is released from the trough to execute cyclotron motion. Thus efficient electron trapping happens only if

$$\tau \gtrsim \tau_{Be} \text{ (electron bounce period)} \lesssim x_v/U \ . \tag{6}$$

Here $\tau_{Be} = 2\pi(m_e/ek^2\phi_o)^{1/2}$ is the unmagnetized bounce period and a justification of its use is that for $|x| \leq x_v$ wave electric force dominates over the magnetic force. The condition $\tau \gtrsim \tau_{Be}$ requires

$$e\phi_o \gtrsim m_e v^2 \tag{7}$$

while $x_v/U \gtrsim \tau_{Be}$ requires

$$e\phi_o \gtrsim m_e U^2(\omega_{ce}/\omega)^{4/3} \tag{8}$$

The required trapping potential is hence the larger one of the above two values. In the case here with $\omega \sim \omega_{UH}$ we have $e\phi_{tr} \sim m_e U^2$; that is,the trapping potential is the same as if the magnetic field were absent. It is interesting to note that for a low-frequency ($\omega < \omega_{ce}$) wave the required trapping potential is

$(\omega_{ce}/\omega)^{4/3}$ times larger than that without $\vec{B}_o$. With relation (6) satisfied, an electron will then be trapped inside a wave trough and carried by the wave to climb up the magnetic force potential until $x \simeq x_v$. At $x \simeq x_v$, the combined potential trough vanishes and this trapped electron is released with an increased kinetic energy

$$\frac{1}{2} m_e v_{rel}^2 = \frac{1}{2} m_e (\omega_{ce} x_v)^2 \sim \frac{1}{2} m_e U^2 \quad . \tag{9}$$

For Maxwellian electrons and $U >> v_e$, therefore, it is expected that the bulk of the electron population will be trapped when, phenomenologically,

$$e\phi_{e,s} = \frac{1}{4} m_e U^2 \quad . \tag{10}$$

Since at $e\phi_{e,s}$, $\tau_{Be} \sim \omega_{UH}^{-1} << \omega_{im}^{-1} \sim \omega_{pi}^{-1}$ the linear instability will be stabilized by the significant number of electrons executing nonlinear trapping orbits inside the troughs. Meanwhile, the electron perpendicular temperature at the saturation will be

$$\frac{T_{e\perp,s}}{T_{o\perp}} = (U/v_e)^2 \tag{11}$$

Since $\frac{\tau_{ce}}{x_v/U} \sim \omega_{UH}/\omega_{ce} = 1.4 \sim 1$ and the released electrons execute cyclotron motions, the velocity distribution will be roughly isotropic.

As to the effectively unmagnetized ions, the usual trapping arguments predict ion trapping when

$$e\phi_{i,s} = \frac{1}{4} m_i (\omega_{rm}/k_m - U)^2 \quad . \tag{12}$$

Using (2) and (9), we have

$$\frac{e\phi_{i,s}}{e\phi_{e,s}} = 0.16 (\omega_{pe}/\omega_{UH})^{2/3} (m_i/m_e)^{1/3} \quad . \tag{13}$$

For $m_i/m_e = 50$ and 100, $e\phi_{i,s}/e\phi_{e,s} \sim 0.35$ and ions, therefore, will be trapped before the electrons. However, $\tau_{Be}/\tau_{Be} = (m_i/m_e)^{1/2}$ and trapped electrons execute many more nonlinear bounce oscillations than trapped ions. Therefore it is mainly electron trapping that stabilizes this instability. The wave energy at the saturation then is

$$\frac{\varepsilon_{w,s}}{\bar{n} T_{o\perp}} \simeq \frac{\varepsilon_o k^2 e^2 \phi_{e,s}^2}{\bar{n} m_e v_e^2} = \frac{1}{16} (\omega_{UH}/\omega_{pe})^2 (U/v_e)^2 = 0.13(U/v_e)^2 \quad . \tag{14}$$

Fig. 15 plots the measured $(\varepsilon_{w,s}/\bar{n} T_{o\perp})^{1/2}$ and $(T_{e\perp,s}/T_{o\perp})^{1/2}$ versus $E_o/B_o v_e$. The agreements with (11) and (14) are rather good, considering the many uncertain constants involved.

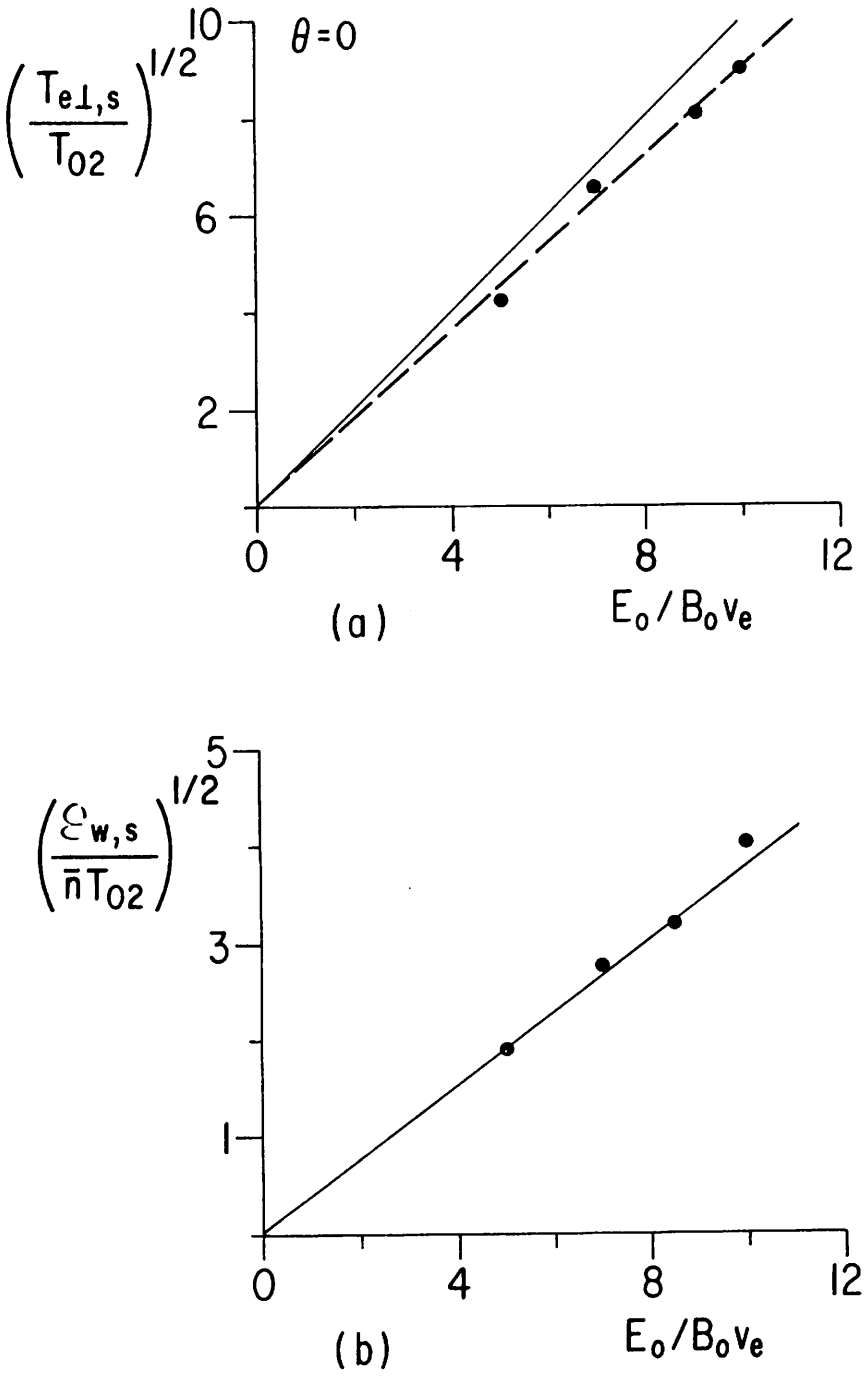

Fig. 15 Plots of the measured (a) $(T_{e\perp s}/T_{o\perp})^{1/2}$ and (b) $(\varepsilon_{w,s}/\bar{n}\, T_{o\perp})^{1/2}$ vs. $E_o/B_o v_e$. Here $\theta = 0$. The solid lines indicate the theoretically estimated values.

Since heating is a consequence of particle trapping, simulation results suggest that a possible explanation for the smallness of the observed ion heating is due to the large ratio, τ_{Bi}/τ_{Be}. Therefore a rough estimate of ion temperature at the saturation is

$$\frac{T_{i\perp,s}}{T_{o\perp}} \simeq \frac{T_{e\perp,s}}{2T_{o\perp}} \left(\frac{m_e}{m_i}\right)^{1/2} , \tag{15}$$

which gives values in the same orders of magnitudes as the measured values.

b. Modified two-stream instability. In this instability electrons mainly move along the magnetic field and, for $\theta^2 << 1$, can be considered as having an effective mass, $\bar{m}_e = m_e/\theta^2$. Corresponding to experiment (c), numerical solutions of the dispersion relation indicate that the fastest growing mode has

$$\begin{aligned} \omega_{rm} &= 1.54\ \omega_{pi} \\ k_m U &= 2.2\ \omega_{pi} \end{aligned} \tag{16}$$

and hence a phase velocity 0.7 U in the electron frame. Since B_o does not affect parallel motions, electron trapping potential is

$$e\phi_{e,s} = \frac{1}{4}\bar{m}_e \ (\omega_{rm}/k_m)^2 = 2\ m_e\ U^2 \ . \tag{17}$$

For ions we have

$$e\phi_{i,s} = \frac{1}{4}\ m_i\ (\omega_{rm}/k_m - U)^2 = 2.5\ m_e\ U^2 \tag{18}$$

Thus $e\phi_{i\ s}/e\phi_{e\ s} \sim 1$, and electrons and ions get trapped at about the same time; this is in contrast with the early case where $e\phi_{i,s} < e\phi_{e,s}$ and ions get trapped first. Furthermore, because $\tau_{Bi}/\tau_{Be} = (m_i/\bar{m}_e)^{1/2} \simeq 2.4$ electrons are still more "responsible" for saturating the instability than the ions. The ions, however, play a more important role in the stabilizing process than in the earlier case where $\tau_{Bi}/\tau_{Be} \sim 10$. From (17) the electrostatic field energy at the saturation then is about 2 times higher than the earlier value

$$\frac{\varepsilon_{w,s}}{\bar{n}\ T_{o\parallel}} \simeq 0.4\ (U/v_e)^2 \ . \tag{19}$$

Meanwhile, the parallel electron temperature at saturation is expected to be

$$\frac{T_{e\parallel,s}}{T_{o\parallel}} = \bar{m}_e\ (\omega_{rm}/k_m)^2 = 8\ (U/v_e)^2 \ . \tag{20}$$

Again, $\tau_{Bi}/\tau_{Be} \simeq 2.4$ suggests an estimate of ion temperature is

$$\frac{T_{i,s}}{T_{o\parallel}} \simeq \left(\frac{T_{e\parallel,s}}{T_{o\parallel}}\right)\left(\frac{\bar{m}_e}{m_i}\right)^{1/2} = 3.3\ (U/v_e)^2 \ . \tag{21}$$

Fig. 16 shows $(\varepsilon_{w,s}/\bar{n}\, T_{o\parallel})^{1/2}$, $(T_{e\parallel,s}/T_{o\parallel})^{1/2}$ and $(T_{i,s}/\bar{n}\, T_{o\parallel})^{1/2}$ for $E_o/B_o v_e = 5$ and 7. Although the data are insufficient to completely confirm the above estimates, they appear to suggest that the temperature estimates are reasonably good; the actual values of $\varepsilon_{w,s}$ are about twice large than the estimated values. (The whole procedure was only meant to be an estimation anyway.) Since $\omega << \omega_{ce}$, $kr_e << 1$ and electron trapping is dominantly in the parallel direction, electron motion in the perpendicular plane is then mainly the $\vec{E}_w x \vec{B}_o$ drift.

For both instabilities, the post-saturation period is characterized by further thermalizations of the particles accompanied by gradual smearings in the phase spaces as well as the disappearances of sharp peaks in the wave spectra. So far we have developed no clear understanding about this part of the heating cycle.

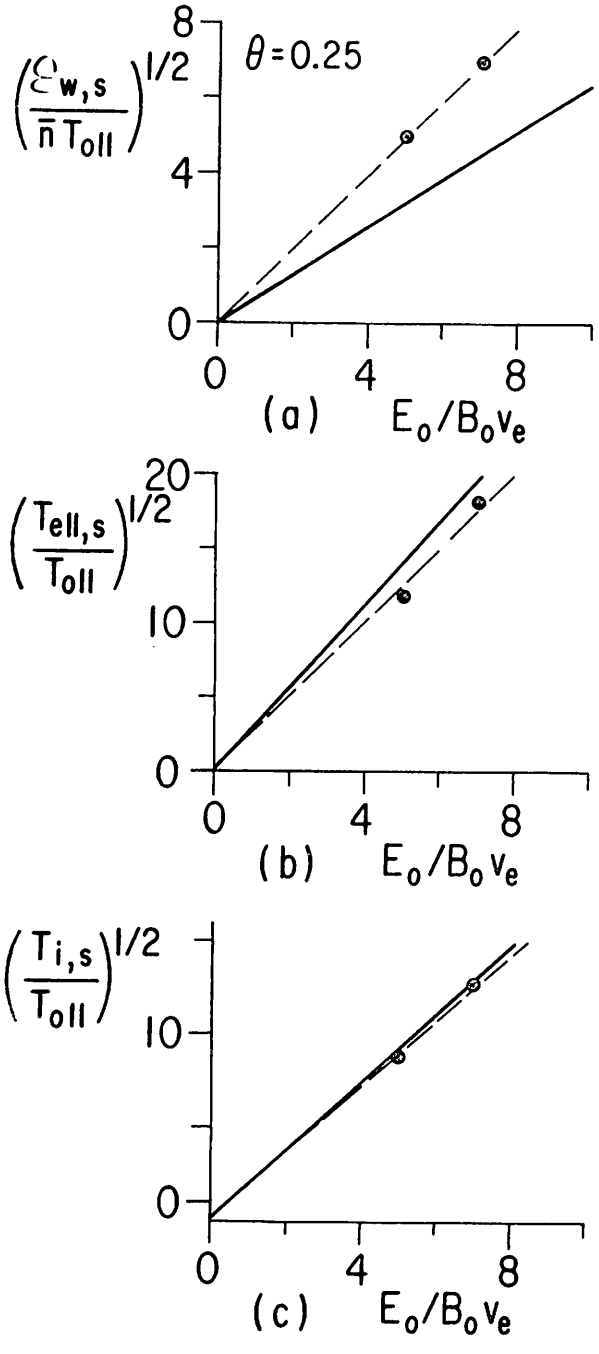

Fig. 16 Plots of the measured (a) $(\varepsilon_{w,s}/\bar{n}\, T_{o\parallel})^{1/2}$, (b) $(T_{e\parallel,s}/T_{o\parallel})^{1/2}$ and (c) $(T_{i,s}/T_{o})^{1/2}$ vs. $E_o/B_o v_e$. Here $\theta = 2.5\,(m_e/m_i)^{1/2} = 0.25$. The solid lines indicate the theoretically estimated values.

VI. COMPARISON OF HEATING WITH AND WITHOUT B_o

As the heating without B_o has already been investigated in simulation by Kruer et al., it is desirable to compare their results with those with B_o. This Section is only a cursory comparison, not meant to be exhaustive.

In both simulations, the heating is done by a large-amplitude E_o applied at frequency $\omega_o \simeq \omega_{pi}$. The major comparisons sought are (1) the threshold values of E_o needed to excite the instability and (2) the value of nKT_e, nKT_i at wave saturation. The results show that ion heating is largest with B_o present and the modified two-stream instability excited. The details of the various heatings are shown in Table 2, which will now be described.

For $B_o=0$, the simulation of Kruer et al.[16] shows that the ordinary two-stream instability is excited and at wave saturation the electron thermal velocity reaches the maximum drift velocity (i.e., $KT_{e,s} \simeq m_e(eE_o/m_e\omega_o)^2$, or $nKT_{e,s} \simeq (m_i/m_e)\varepsilon_o E_o^2$ with $\omega_o \simeq \omega_{pi}$ as given in the table). The ion thermal velocity at wave saturation is estimated to be $v_{i,s} \simeq (eE_o/m_e\omega_o)(m_e/m_i)^{3/4}$ from $T_{i,s}/T_{e,s} \simeq \tau_{Bounce,e}/\tau_{Bounce,i}$; which quantatively agrees with the result given by Kruer et al., in their Fig.1. The threshold value of E_o here is $E_{o,thresh} \simeq v_{e,initial} \cdot (m_e\omega_{pi}/e) \simeq B_o v_{e,initial}(\omega_{pi}/\omega_{ce})$, for use later where $B_o \neq 0$.

For $B_o \neq 0$ and $\theta \lesssim (m_e/m_i)^{1/2}$, we have found that the upper-hybrid two-stream instability is excited. At wave saturation, electron

TABLE 2. Summary of various heating results using large-amplitude low-frequency electric field with and without $\vec{B}_o$. If we choose $\theta \simeq m_e/m_i$ for the modified two stream, then the electron and ion temperatures come out to m_i/m_e; the ion heating is better by $\sqrt{m_i/m_e}$ than for $B_o = 0$.

	$B_o = 0$ Ordinary 2-stream-instability	$B_o \neq 0$ $\theta \leq \sqrt{\frac{m_e}{m_i}}$ upper-hybrid 2-stream instability	$B_o \neq 0$ $1 > \theta > \sqrt{\frac{m_e}{m_i}}$ modified 2-stream instability
Driving Frequency ω_o	$\omega_o \simeq \omega_{pi}$		
Maximum drift velocity U_{max}	$\frac{eE_o}{m_e\omega_o}$	$\frac{E_o}{B_o}$	$\frac{E_o}{B_o}$
Threshold conditions	$U_{max} > v_e$	$U_{max} > v_e$	$U_{max} > v_i$
$\varepsilon_o E_{o,thresh}^2/nKT_{e,init}$	$\frac{m_e}{m_i}$	1	$\frac{m_e}{m_i}$
Electron temperature at wave saturation $(nKT_{e,s}/\varepsilon_o E_o^2)$	$\frac{m_i}{m_e}$	perpendicular 1	parallel θ^{-2}
Ion temperature at wave saturation $(nKT_{i,s}/\varepsilon_o E_o^2)$	$\sqrt{\frac{m_i}{m_e}}$	(perpendicular) $\sqrt{\frac{m_e}{m_i}}$	(Perpendicular) $\sqrt{\frac{m_e}{m_i}}\,\theta^{-3}$

$E_{ext} = E_o \sin \omega_o t$. $\omega_{pe} \simeq \omega_{ce}$. Initially, $m_e v_e^2 \simeq m_i v_i^2$.

perpendicular thermal energy is increased to $nKT_{e\perp,s} \simeq \varepsilon_o E_o^2$ and $nKT_{i\perp,s} \simeq (m_e/m_i)^{1/2} \varepsilon_o E_o^2$. Here we have assumed $\omega_{pe} \simeq \omega_{ce}$. In this case, $E_{o,thresh} \simeq B_o v_{e,initial}$.

For $B_o \neq 0$ and $1 > \theta > (m_e/m_i)^{1/2}$, our simulations show that the modified two-stream instability is excited. At wave saturation, electron parallel thermal energy is increased to $nKT_{e\parallel,s} \simeq \varepsilon_o E_o^2 \theta^{-2}$ and ion (perpendicular) temperature increased to $nKT_{i,s} \simeq \varepsilon_o E_o^2 \theta^{-3} \cdot (m_e/m_i)^{1/2}$. Here, again, we have assumed $\omega_{pe} \simeq \omega_{ce}$. If we, optimistically, assume $\theta \simeq \sqrt{m_e/m_i}$, we then have $nKT_{e\parallel,s} \simeq nKT_{i,s} \simeq (m_i/m_e) \cdot \varepsilon_o E_o^2$. The corresponding $E_{o,thresh}$ is about $B_o v_{i,intial} \simeq B_o v_{e,initial} \cdot (m_e/m_i)^{1/2} \simeq B_o v_{e,initial} (\omega_{pi}/\omega_{ce})$ for $m_e v_{e,initial}^2 \simeq m_i v_{i,initial}^2$ and $\omega_{pe} \simeq \omega_{ce}$.

From the point of view of maximum temperature obtained at wave saturation, we see the following comparisons:

(a) For $B_o = 0$, the electrons are heated more than the ions by a factor of $(m_i/m_e)^{1/2}$, implying production of a hot electron plasma.

(b) For $B_o \neq 0$ and the upper-hybrid two-stream instability excited, the heating is smaller by a factor of $\sqrt{m_e/m_i}$ for both electrons and ions than the $B_o = 0$ case.

(c) For $B_o \neq 0$ and the modified two-stream instability excited, the electron heating is the same as in the $B_o = 0$ case, but the ion heating is $(m_i/m_e)^{1/2}$ times better and $T_{e,s} \simeq T_{i,s}$.

(d) As to the threshold value of E_o, the heating with $B_o \neq 0$ and upper-hybrid two-stream instability excited requires a value $(m_i/m_e)^{1/2}$ times larger than that for the $B_o = 0$ case as well as the

case with $B_o \neq 0$ and the modified two-stream instability excited. The threshold values of E_o for the $B_o=0$ and the modified two-stream instability heatings are about the same .

Hence, based on the conditions chosen, it appears that much more effective ion heating can be obtained by adding the steady magnetic field and ensuring that the modified two-stream instability is excited. The advantage is roughly $(m_e/m_i)^{1/2}$ in ion heating over the $B_o \neq 0$ case, an advantage well worth taking.

It is also worthwhile to put in some numbers in order to get a feeling for the magnitudes involved. Taking a gaseous deuterium plasma with $n \simeq 10^{14}$ (cm^{-3}) and $\sqrt{m_i/m_e} \simeq 60$, then the driving frequency required is $f_o \simeq f_{pi} \simeq 1.5 \times 10^9$ Hz. The condition that $\omega_{pe} \simeq \omega_{ce}$ means $B_o \simeq 30$ kG. In order to heat the ions, the modified two-stream instability heating is chosen, which produces $nKT_i \simeq (m_i/m_e)\varepsilon_o E_o^2$ at wave saturation. Using $KT_i \simeq 10$ keV, this requires $\varepsilon_o E_o^2 = 10^5$ Joules/m^3 or $E_o = 10^8$ V/m $(=10^6$ V/cm). Since the heating is generally accomplished within several ion plasma periods, say, $5\tau_{pi}$; the required pulse duration is roughly 3×10^{-9} sec. This implies delivering 10^5 Joules/m^3 in 3×10^{-9} sec or about 3×10^{13} Watts per cubic meter of plasma (3×10^7 Watts per cm^3). The next steps (not taken here) would be to choose a possible pulsed reactor size and configuration, working out method of producing E_o within the plasma (by electron beam or wave propagation); however, without these answers it still appears that these parameters ($E_o \sim 10^6$ V/cm, $B_o \sim$ 30 kG, $f_o \sim 1.5$GHz, plasma size not clear) are not terribly beyond present capabilities.

VII. CONCLUSIONS AND DISCUSSIONS

We have shown with one-dimensional computer simulations that a large-amplitude ($E_o/B_o > v_e$) low-frequency ($\omega_o \sim \omega_{pi}$) electric field $\vec{E}_{ext} = \vec{E}_o \sin \omega_o t$ when applied across a constant magnetic field $\vec{B}_o$ can efficiently heat the plasma (electrons as well as ions) to high temperatures. The heatings are the results of instabilities excited by the electron $\vec{E}_{ext} \times \vec{B}_o$ oscillating drift through the ions. The plasmas considered here are Maxwellian, with initial $T_e \simeq T_i$ and $\omega_{pe} = \omega_{ce}$.

For waves propagating perpendicularly to B_o ($\theta \sim \frac{k_\parallel}{k} = 0$), Buneman-type upper-hybrid two-stream instability ($kE_o/B_o \sim \omega_{UH}$) is excited. This instability has periodic growth with maximum growth when the drift speed is near its peak value E_o/B_o. As the wave energy increases, electrons become trapped and their perpendicular (to $\vec{B}_o$) thermal speed is rapidly increased to $\sim E_o/B_o$. While the ions are also trapped, their perpendicular temperature is relatively small, about $(m_e/m_i)^{1/2}$ that of the corresponding electron value.

For waves propagating obliquely to B_o ($\theta \neq 0$), the ions are treated as unmagnetized in the simulations and in addition to the upper-hybrid two-stream instability the modified two-stream instability emerges at low wave numbers ($k E_o/B_o \sim \omega_{pi}$). This instability has nearly a constant exponential growth due to its low threshold, $\sim v_i$. As θ increases, the maximum growth rate as well as the spectrum width (in k) of the modified two-stream instability increase. These properties of the upper-hybrid two-stream

instability, however, have little change. Thus, with θ small (roughly $\theta \lesssim \sqrt{m_e/m_i}$) the upper-hybrid two-stream instability still dominates and the dynamics are rather similar to the $\theta = 0$ case with little electron heating in the parallel direction. As θ becomes larger, however, the modified two-stream instability becomes dominant. For this instability electrons mainly respond in the parallel direction and can be thought of as having an effective mass, $\bar{m}_e = m_e/\theta^2$. As the waves get stronger, electrons become trapped in the parallel direction and their parallel thermal speed is increased to $\sim 0,7\ E_o/B_o\ \theta \sim 0.7\ (k/k_{\parallel})\ (E_o/B_o)$ for $\theta = 2.5\ (m_e/m_i)^{1/2}$. Ion "perpendicular" heating is about $(\bar{m}_e/m_i)^{1/2}$ of the electron parallel heating.

We also compare the above heating results with $B_o \neq 0$ with those of $B_o = 0$. The comparisons indicate that ion heating is largest if $B_o \neq 0$ and the modified two-stream instability is excited.

In real laboratory experiments, waves propagating in all directions can be excited. Because the modified two-stream is active for a range of θ wider than the upper-hybrid instability, and its maximum growth rate increases with increasing θ at least when $\theta << 1$, it therefore, is expected to be dominant over the upper-hybrid two-stream instability. Thus, efficient electron parallel and ion heating can be expected. That electron heating is mainly in the parallel direction might be a problem for mirror confinement.

Since the instabilities discussed here are excited by large-amplitude drifts and not by parametric effects, we expect the results obtained here with $\omega_o = \omega_{pi}$ to hold also for ω_o's other than ω_{pi} ; that is, the pump frequency need not be finely tuned as in parametric excitations. This expectation, however, remains to be verified.

ACKNOWLEDGMENTS

We are thankful to Professor Allan N. Kaufman for his valuable comments.

This work was supported in part by the United States Atomic Energy Commission, Contract AT-(11-1)-34 (Project 128).

REFERENCES

* Present address: Bell Telephone Labs., Murray Hill, N.J.

1. H. Okuda, J. M. Kindel and J. M. Dawson, Proc. of the 5th Conf. on Numerical Simulations of Plasmas (1971). Also J. M. Kindel, H. Okuda and J. M. Dawson (to be published in Phys. Fluids).

2. C. L. Hsieh, Ph.D. dissertation, University of California, at Berkeley (1972).

   Also, C. L. Hsieh and M. A. Lieberman, Bull. Amer. Phys. Soc. 16, No. 11, 1262 (1971).

3. G. M. Hass and R. A. Dandl, Phys. Fluids 10, 678 (1967). Also, G. M. Hass and M. Eisner, Phys. Fluids 14, 606 (1971).

4. V. P. Bhatnagar and W. D. Getty, Phys. Rev. Lett. 26, 1527 (1971).

   Also, V. P. Bhatnagar, Ph.D. dissertation, Technical Report No. 121, Electron Phys. Lab., University of Michigan (1971).

5. C. K. Birdsall and D. Fuss, J. Comput. Phys. 3, 494 (1969).

6. J. P. Boris, Proc. of the 4th Conf. on Numerical Simulation of Plasmas (1970).

7. J. A. Byers and M. Grewal, Phys. Fluids 13, 1819 (1970).

8. A. B. Langdon, J. Comput. Phys. 6, 247 (1970).

9. O. Buneman, Plasma Phys. (J. Nucl. Energy Part C) 4, 111 (1962).

10. P. Gary, J. Plasma Phys. 6, Part 3, 561 (1971).

11. D. W. Forslund, R. L. Morse and C. W. Nielson, Phys. Rev. Lett. 25, 1266 (1970).

12. M. Lampe, W. M. Manheimer, J. B. McBride, J. H. Orens, K. Papadopoulos, R. Shanny and R. N. Sudan, Phys. Fluids, 15, 662 (1972).

13. N. A. Krall and P. C. Liewer, Phys. Rev. 4, 2094 (1971).

14. E. Ott, J. B. McBride, J. H. Orens and J. P. Boris, Phys. Rev. Lett. 28, 88 (1972).

REFERENCES (Contd)

15. D. W. Forslund, R. L. Morse and C. W. Nielson, Phys. Rev. Lett. 27, 1424 (1971).

Also, in IAEA Conference Paper, 2, 277 (1971).

16. W. L. Kruer, J. Katz, J. Byers and J. DeGroot, MATT-879, Princeton Plasma Physics Laboratory (1972).

Note: Sometimes one wishes to find a name that describes the phenomenon being used, simply to avoid long titles like that of this paper. The process described herein is that of making an oscillatory drift which then sets up an instability, which then causes heating. So, one could name it Drift Instability Heating, DIH. Or, one could call it Heating by Oscillatory Drift, HOD. Indeed, in Webster's Third New International Dictionary, 1964, under "hod", one finds the root of the first meaning to come from "to shake", "to shake up" and the second meaning "to bob up and down". Hence, if a name is to be chosen for this form of heating (e. g., to go along with other forms of heating, like ECRH, electron cyclotron resonance heating), then it is suggested that HOD be used.

APPENDIX 1. Further Descriptions of the Simulation Techniques.

(a) Poisson's Equation. Poisson's equation, in its three-point, one-dimensional difference form is

$$\phi_{j+1}-2\phi_j+\phi_{j-1}=-(\Delta x)^2\rho_j/\varepsilon_o \quad . \tag{A.1}$$

Here j is the index for the grid points and Δx is the distance between two neighboring grid points. The self-consistent electric field then in

$$E_j = -(\phi_{j+1} - \phi_{j-1})/\ 2\Delta x \quad . \tag{A.2}$$

Applying Discrete Fast Fourier Transform to a system with 2N grid points and periodic boundary conditions, we can express ϕ_j and E_j as

$$\left.\begin{aligned} \rho_j &= \sum_{k=0}^{N-1} \tilde{\rho}_c(k)\cos(\pi jk/N) + \tilde{\rho}_s(k)\sin(\pi jk/N), \\ E_j &= \sum_{k=0}^{N-1} \tilde{E}_c(k)\cos(\pi jk/N) + \tilde{E}_s(k)\sin(\pi jk/N); \end{aligned}\right\} \quad j=0,..,2N-1. \tag{A.3}$$

Substituting (A.3) into (A.1) and (A.2), one obtains the following relations

$$E_c(k) = -\frac{\tilde{\rho}_s(k)}{2\tan(\pi k/2N)}\,,$$
$$E_s(k) = \frac{\tilde{\rho}_c(k)}{2\tan(\pi k/2N)}\,; \qquad k=1,\ldots,N-1. \qquad (A.4)$$

In our simulations, we use

$$\tilde{\rho}_s(0) = \tilde{E}_s(0) = \tilde{\rho}_c(0) = \tilde{E}_c(0) = 0.$$

To reduce the short-wave-length noise, we do k-space smoothing by multiplying $\tilde{E}_c(k)$ and $\tilde{E}_s(k)$ with a smoothing function defined as

$$S_m(k) = \exp\left[-(k/k_o)^4\right] \quad ; \quad k = 1,\ldots,N-1. \qquad (A.5)$$

For $\theta = 0$ and $N = 32$, $k_o = 20$. For $\theta \neq 0$ and $N = 64$, $k_o = 35$.

(b) Equation of Motion. The Cylrad Particle Pusher in its general form is

$$\begin{aligned}
\vec{v}_1 &= \vec{v}(t-\Delta t/2) + q\Delta t\vec{E}(t)/2m,\\
\vec{v}_2 &= \vec{v}_1 + f_1\vec{v}_1\times\vec{B}_o,\\
\vec{v}_3 &= \vec{v}_1 + f_2\vec{v}_2\times\vec{B}\,,\\
\vec{v}(t+\Delta t/2) &= \vec{v}_3 + q\Delta t\vec{E}(t)/2m\,;
\end{aligned} \qquad (A.6)$$

where $f_1 = \dfrac{\tan(\omega_{ce}\Delta t/2)}{B}$ and $f_2 = 2f_1/(1+f_1^2B^2)$.

In our one-dimensional model with $\vec{B} = \vec{B}_o$, $\vec{E}_{ext} = E_{ext}\,\hat{y}$ and $\vec{E}_w = E_w\,\hat{x} = E_w \cos\theta\,\hat{x}' + E_w \sin\theta\,\hat{B}_o$ we have using $(\hat{x}', \hat{y}, \hat{B}_o)$ coordinates

$$
\begin{aligned}
v_{x'1} &= v_{x'}(t-\Delta t/2) + q\Delta t E_w \cos\theta\ , \\
v_{y1} &= v_y(t-\Delta t/2) + q\Delta t E_{ext}/2m\ , \\
v_{x'}(t+\Delta t/2) &= \cos(\omega_c \Delta t)\ v_{x'1} + \sin(\omega_c \Delta t)\ v_{y1} + q\Delta t E_w \cos\theta\ /2m, \\
v_y(t+\Delta t/2) &= -\sin(\omega_c \Delta t)\ v_{x'1} + \cos(\omega_c \Delta t)\ v_{y1} + q\Delta t E_{ext}/2m, \qquad \text{(A.7)} \\
v_{\hat{B}_o}(t+\Delta t/2) &= v_{\hat{B}_o}(t-\Delta t/2) + q\Delta t E_w \sin\theta\ /2m\ .
\end{aligned}
$$

(c) Initial Particle Loading. For $\theta = 0$, the 6400 electrons are divided into 32 groups. In each velocity group 200 electrons are used to represent a 2-dimensional isotropic Maxwellian with 25 available speeds. The 32 velocity groups are then uniformly distributed in space. The ion loading is similar to the electron loading except ions are placed on top of electrons so that initial noise is minimized.

For $\theta \neq 0$, the 14000 electrons are divided into 35 velocity groups. In each group 400 electrons are used to represent a 3-dimensional isotropic Maxwellian with 25 available speeds. The 35 velocity groups are distributed uniformly across the system. For the 6060 ions, there are 60 velocity groups; that is, 101 ions

are used to represent a 1-dimensional Maxwellian. The ions are then distributed uniformly in space.

In our simulations, the initial fluctuations are rather small, $\varepsilon_w(0)/\bar{n}KT(0) \simeq 0(10^{-3})$. Although E_{ext} is applied at $t = 0$ when the plasma is not at thermal equilibrium, however, since the driving field is so strong that we expect the results will have little difference from those with E_{ext} applied when the plasma is at true thermal equilibrium.

APPENDIX 2. Further Discussions on the Upper-Hybrid and Modified Two-Stream Instabilities.

In this Appendix we analyze the dispersion relation in more detail and show the results cited in Section V.

(a) Upper-hybrid two-stream instability. The corresponding dispersion relation is

$$1 - \frac{\omega_{pe}^2}{\omega^2-\omega_{ce}^2} - \frac{\omega_{pi}^2}{(\omega - kU)^2} \simeq 0 \quad . \qquad (3)$$

This instability, therefore, arises due to the interaction between the ion beam mode and the electron upper-hybrid oscillation: $\omega = \omega_{UH}$. As shown by Buneman,[10] in this instability ions can be treated as if they had an effective mass $\bar{m}_i = m_i\, \omega_{pe}/\omega_{UH}$. With the effects of the magnetic field absorbed in $\bar{m}_i$, we then can, in analogue to the usual two-stream instability, obtain the relations expressed in (4).

Let us check the conditions on the validity of the fluid approximations. The condition $k\, v_e/\omega_{ce} < 1$ requires

$$v_e/U < \omega_{ce}/\omega_{UH} \sim 1 \text{ for } \omega_{ce} \geq \omega_{pe}. \qquad (A.8)$$

The condition $|\omega/k - U| > v_i$ requires

$$v_i/U < (m_e/m_i)^{1/3}\, (\omega_{pe}/\omega_{UH})^{4/3} \quad . \qquad (A.9)$$

Corresponding to our simulation; $m_e V_e^2 \sim m_i V_i^2$ and $\omega_{pe} \sim \omega_{ce}$, we have (A.9) as

$$v_e/U < (m_i/m_e)^{1/6}\, (\omega_{pe}/\omega_{UH})^{4/3} \quad . \qquad (A.9)'$$

(b) Modified two-stream instability. The corresponding dispersion relation is

$$\frac{\omega_{UH}^2}{\omega_{ce}^2} - \frac{\omega_{pe}^2}{\omega^2}\sin^2\theta - \frac{\omega_{pi}^2}{(\omega-kU)^2} = 0 \; ; \qquad (5)'$$

which can also be written as

$$1 - \frac{\bar{\omega}_{pe}^2}{\omega^2} - \frac{\bar{\omega}_{pi}^2}{(\omega-kU)^2} = 0 \quad . \qquad (A.10)$$

Here, for $\omega_{ce} \geq \omega_{pe}$, $\bar{\omega}_{pe}^2 = \omega_{pe}^2 \sin^2\theta(\omega_{ce}/\omega_{UH})^2 \simeq \omega_{pe}^2 \sin^2\theta$ and $\bar{\omega}_{pi}^2 = \omega_{pi}^2 (\omega_{ce}/\omega_{UH})^2 \sim \omega_{pi}^2$. Therefore, this instability arises due to the interaction between the ion beam mode and a modified electron plasma oscillation: $\omega = \bar{\omega}_{pe} \sim \omega_{pe} \sin\theta$ Furthermore, (A.10) is the same as the dispersion relation for the usual two-stream instability with an effective electron mess $\bar{m}_e = m_e/\sin^2\theta = m_e (k/k_{\parallel})^2$; and, therefore, we can expect the following relations

$$\omega_i \sim |\omega-kU| \sim \bar{\omega}_{pe} (\bar{m}_e/m_i)^{1/3} \sim \omega_{pe}(m_e/m_i)^{1/3}(k_{\parallel}/k)^{1/3} \qquad (A.11)$$

and

$$\omega \sim kU \sim \omega_{pe} (k_{\parallel}/k). \qquad (A.12)$$

(A.11) contains the dependence of growth rate on the angle $\theta = \sin^{-1}(k_{\parallel}/k) \sim k_{\parallel}/k$.

From (A.11) and (A.12), the conditions on the fluid approximations are for $k\, r_e/\omega_{ce} < 1$

$$\frac{v_e}{U} < \frac{k}{k_{\parallel}} \cdot \frac{\omega_{ce}}{\omega_{pe}} \quad ; \tag{A.13}$$

for $\omega/k_{\parallel} > v_e$

$$\frac{v_e}{U} < \frac{k}{k_{\parallel}}$$

and for $|\omega - kU| > v_i$.

$$\frac{v_i}{U} < (m_e/m_i)^{1/3} \, (k/k_{\parallel})^{2/3} \tag{A.14}$$

with $k_{\parallel}/k \sim (m_e/m_i)^{1/2}$, (A.14) then becomes $\frac{v_i}{U} < 1$.